JOURNAL OF GEOPHYSICAL RESEARCH, VOL. 96, NO. C8, PAGES 14,927–14,945, AUGUST 15, 1991

Water Mass Subduction and the Transport of Phytoplankton in a Coastal Upwelling System

LIBE WASHBURN,[1,2] DAVID C. KADKO,[3,4] BURTON H. JONES,[1] THOMAS HAYWARD,[5] P. MICHAEL KOSRO,[3] TIMOTHY P. STANTON,[6] STEVE RAMP,[6] AND TIMOTHY COWLES[3]

Observations during the Coastal Transition Zone (CTZ) experiment in summer 1988 reveal the presence of deep phytoplankton layers in a coastal upwelling system. The layers occur throughout the CTZ study area, including a strong baroclinic jet which was present over the period of the experiment. On the basis of a variety of bio-optical, hydrographic, and geochemical indicators, it is concluded that the water masses associated with the layers result from subduction processes. Criteria are developed for identification of subducted water masses based on the beam attenuation coefficient, chlorophyll fluorescence, and distribution of light in the water column. Temperature-salinity characteristics are consistent with two source regions for the subducted layers, one nearshore and a second farther offshore. Most of the layers correspond to the inshore source which is apparently distributed alongshore. Subducted water masses are found in all six grid surveys of the CTZ experiment and probably result from a variety of physical processes. One of these is flow along sloping isopycnal surfaces due to advection and mixing processes. Advection time scales for flow out the axis of the jet range from a few days to a few weeks, depending on the depth of a particular surface, and the bio-optical indicators for subduction processes persist over these time scales.

1. INTRODUCTION

An unanticipated observation during the Coastal Transition Zone (CTZ) experiment is the occurrence of layers of high concentrations of phytoplankton at depths often greatly exceeding the euphotic zone. These layers are found both nearshore and offshore within a productive coastal upwelling system off northern California and are often observed in a strong offshore jet that was present in the CTZ study area in 1988. We explore the hypothesis that the water masses associated with these layers originate near the surface in the euphotic zone and are subsequently transported downward by vertical circulation processes or subduction (other terms such as subsidence or downwelling are equally descriptive). The subduction hypothesis is supported by a variety of physical, biological, and geochemical indicators including ^{222}Rn, dissolved O_2, and chlorophyll *[Kadko et al.,* this issue].

The movement of large volumes of water out of the surface layer (euphotic zone) is potentially important to the vertical transport of heat, mass, salt, and other scalars. Furthermore, geochemical data indicate that this transport can be rapid with vertical velocities of the order of 20–30 m d^{-1} *[Kadko et al.,* this issue]. It also may result in a high vertical flux of organic carbon, and it represents a mechanism which could quickly remove large concentrations of phytoplankton from the euphotic zone in a productive coastal environment.

At this point, the characteristics of subducted water masses and the mechanisms leading to their subduction in a coastal region are not well understood. Some basic questions include, What are the thicknesses, horizontal extents, and volumes of subducted water masses? Are subducted water masses only associated with offshore jets or are they more widely distributed in the CTZ? Where are the source regions for the subducted water masses? Are the source regions local in the sense that subduction results form vertical sinking with little horizontal advection? Or, is horizontal advection strong enough to move subducted water masses away from the region where sinking occurs? Are subducted waters transported offshore and, if so, at what rates? What physical processes lead to subduction?

Experimentally, it is necessary to determine quantities and criteria that can be used to establish that an observed water mass has been subducted. It is also important to determine the effective decay times for various subduction indicators.

2. EXPERIMENTAL PROCEDURE

A more complete description of the shipboard observations from the CTZ experiment during summer 1988 is presented by *Huyer et al.* [this issue]. Basically, the overall strategy was to sample a region of the CTZ between Point Reyes and Point Arena, California, over a period of several weeks in order to observe the evolution of strong coastal jets which have been observed previously in the area [cf. *Flament et al.,* 1985; *Davis,* 1985]. To do this, six hydrographic grid surveys of more or less uniform spatial coverage were made sequentially from three ships: R/Vs *Wecoma*, *Point Sur,* and *Thomas Washington* (leg 1). (The sampling grids for five of these surveys are indicated in Figure 4.) Because of adverse weather conditions, the entire leg 1 grid survey from the *Thomas Washington* could not be completed (This incomplete grid is shown in Figure 13). However, the inshore part was completed and is used here to examine nearshore water properties. In addition, during leg 2 of the *Thomas Washington* survey, sampling was specifically di-

[1]University of Southern California, Los Angeles.
[2]Now at Department of Geography, University of California, Santa Barbara.
[3]College of Oceanography, Oregon State University, Corvallis.
[4]Now at Rosenstiel School for Marine and Atmospheric Science, University of Miami, Miami, Florida.
[5]Scripps Institution of Oceanography, La Jolla, California.
[6]Department of Oceanography, Naval Postgraduate School, Monterey, California.

Paper number 91JC01145.
0148-0227/91/91JC-01145$05.00

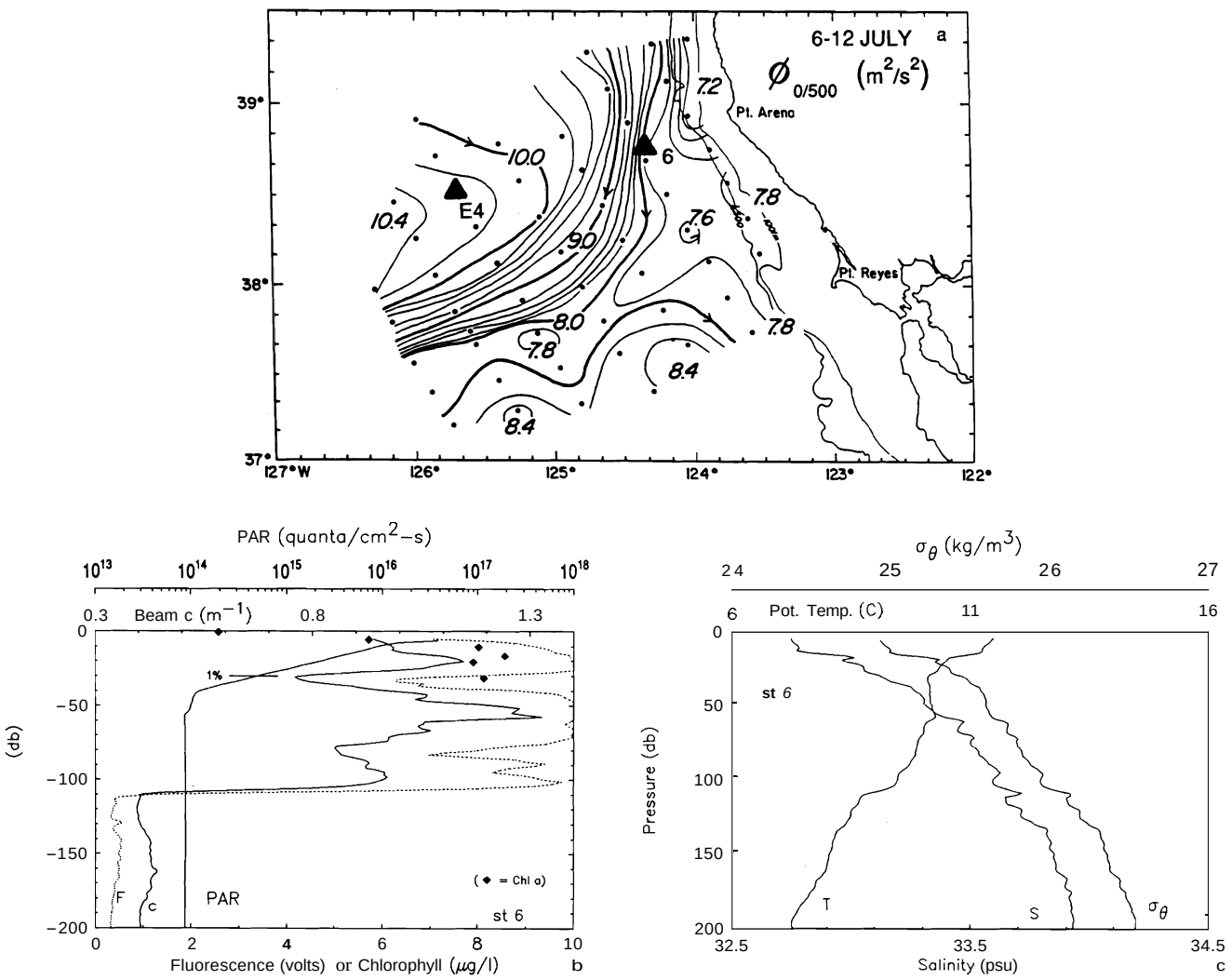

Fig. 1. ***(a)*.Locations of stations E4 and *6*. Contours of geopotential anomaly (01500 dbar) are from the first *Point Sur* survey, July *6–12*, 1988. (*b*) Profiles of photosynthetically available radiation (PAR), beam c, and fluorescence at station 6 along with chlorophyll concentrations at discrete depths from bottle samples. (*c*) Profiles of potential temperature, potential density, and salinity, at station *6*.**

rected at observing physical, biological, and chemical distributions in the offshore jet with some limited sampling outside the jet (station locations are indicated by triangles in Figure 5). The period of this "process sampling" was 18 days (July *4* to July *21)* and coincided with the first two hydrographic grid surveys of the ***Point Sur*** which were conducted from July *6* to 18.

Measured variables from all vessels include conductivity, temperature, depth, chlorophyll fluorescence, beam transmission and meteorological observations. Fluorometers and transmissometers were manufactured by Sea Tech, Inc., of Corvallis, Oregon, and each transmissometer has a 0.25-m path length with a 660-nm-wavelength light source. Rosettes with Niskin bottles were used in conjunction with the conductivity-temperature-depth (CTD) instrumentation to provide bottle sampling for salinity calibration, dissolved O_2, nutrients, chlorophyll, and pigments. Continuous profiles of photosynthetically available radiation (PAR) were made from the ***Thomas Washington*** using a sensor manufactured by Biospherical Instruments, Inc., of San Diego, California.

3. Evidence for Subduction

The primary evidence for subduction processes discussed here is layers of phytoplankton which are observed at depths below the euphotic zone. Because phytoplankton are green plants, they require light for photosynthesis and grow in the illuminated layers of the upper ocean. The presence of phytoplankton in the water column is detected by a combination of chlorophyll fluorescence and beam attenuation coefficient (beam *c*) profiles. Beam c is a quantitative measure of water column turbidity which depends upon various aspects of the particle field such as particle concentrations, size distribution, and index of refraction [cf. ***Jerlov, 1976; Baker and Lavelle,*** 1984]. Vertical profiles of beam c and chlorophyll fluorescence at stations containing phytoplankton layers are highly correlated, and the presence of phytoplankton in these layers is verified by bottle samples. Such a station (station 6), located *50* km west of Point Arena and in a region of strong southward flow, is shown in Figure *la*.

Beam c values exceed *0.4* m^{-1}, and the chlorophyll fluorescence signal is above the noise level almost every-

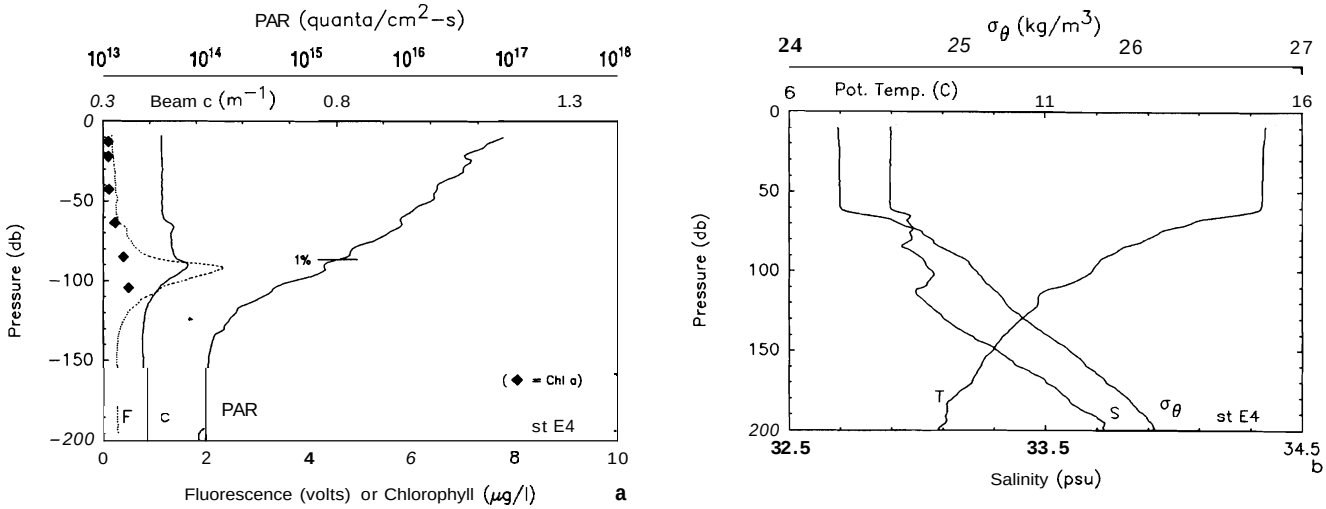

Fig. 2. (a) As in Figure 1*b*, but for station E4. (*b*) As in Figure 1*c*, but for station E4.

where above 190 dbar (Figure lb). The measured 1% light level here is 31 dbar, and three distinct layers are found: (1) a near-surface layer above the 1% light level where chlorophyll concentrations are as high as 8.6 mg L^{-1}, (2) a deeper layer which extends from the 1% light level to about 110 dbar, and (3) a very deep layer with low beam c and and fluorescence levels which extends from 125 to 190 dbar. No surface mixed layer is observed, and gradients in all measured quantities extend to the surface. A weak temperature inversion is present on the upper boundary of layer 2 (Figure 1*c*) and suggests that this layer is intrusive, a conclusion also supported by the potential temperature-salinity (θ-S) diagram for this station. Examples of several 0-S diagrams showing an association between deep fluorescence layers and relatively warm, salty anomalies are given by Kadko *et* al. [this issue].

A very different type of profile is typically found in offshore waters away from the jet, such as at station E4 (Figure 1a). A deep fluorescence layer is centered at about 98 dbar, well below the 60-dbar deep surface mixed layer, and lies just below the 1% light level at 85 dbar (Figure 2*a* and 26). Chlorophyll concentrations from bottle samples are about 0.5 mg L^{-1} just above and below the fluorescence peak; apparently the peak itself was missed in sampling. However, chlorophyll and fluorescence are highly correlated and nearby stations show peak concentrations of about 1 mg L^{-1}. Chlorophyll layers of this type, which occur in association with the base of the euphotic zone, are common features of the California Current system [cf. Anderson, 1969; *Cullen*, 1982]. They may result from a number of processes such as an increase in phytoplankton biomass due to growth at the intersection of the euphotic zone and nutricline [Herbland and Voituriez, 1979]. Two other possibilities are photoadaptation, where the chlorophyll per cell increases in response to low light conditions [Prezelin, 1981; Beers et al., 1975], or variability in fluorescence yield of the phytoplankton [Kiefer, 1973]. At station E4 and nearby stations the increase in beam c indicates increased biomass, while the fluorescence per unit chlorophyll, or fluorescence yield, is relatively constant throughout the water column. However, the chlorophyll per unit beam c increases with depth at E4 and suggests that the chlorophyll content per cell or per unit biomass also increases with depth.

To objectively examine CTZ data sets for the occurrence of phytoplankton layers which may have been moved out of the euphotic zone by subduction processes, it is necessary to differentiate the deep layers like those of Figure 1 from those which probably result from in situ photosynthesis as in Figure 2. Furthermore, it is necessary to rule out other processes which might also result in the presence of layers of fluorescent particles below the euphotic zone. A step in this process is to establish the relationship between the light field in the water column throughout the region and the vertical positions of layers of phytoplankton.

The penetration of light into the water column is examined by comparing vertical profiles of PAR throughout the CTZ. A total of 17 stations from legs 1 and 2 of the Thomas Washington survey, all recorded within one hour of local noon, are used to examine the variability of the light field (Figure 3*a*). Stations close to local noon were chosen in order to observe the maximum penetration of light into the water column. Following Huyer et al. [this issue], three regions are identified based on dynamic height (5/500 dbar): the jet corresponds to the range 0.82–0.96 m, inshore and southern waters below 0.82 m, and offshore and northern waters greater than 0.96 m. These ranges are somewhat different from those used by Huyer et al. [this issue] but are more appropriate to the Thomas Washington data. Considerable variation in the depth of light penetration is found within the jet waters: typical values of the 1% light level in the most turbid waters are in the range of 20 to 30 dbar and are almost 80 dbar in the more clear waters (Figure 36). This depth range also spans that observed for the inshore and southern waters. Offshore waters are generally more clear, with a typical 1% light level of about 85 dbar; much of the phytoplankton in the water column lies below this level.

Observations obtained during leg 2 of the Thomas Washington survey show that almost one fourth of the water column with high chlorophyll fluorescence levels (>1.0 V) is found at depths below the 1% light level of the clearest offshore waters (Figure 3*c*). About 6.4% occurs below the 0.1% light level, which ranges from about 115 to 125 dbar on the basis of the three offshore profiles of Figure 36. The threshold fluorescence value of 1.0 V is chosen because it represents a high signal level; the noise level of the fluorometer and CTD acquisition system used on the Thomas

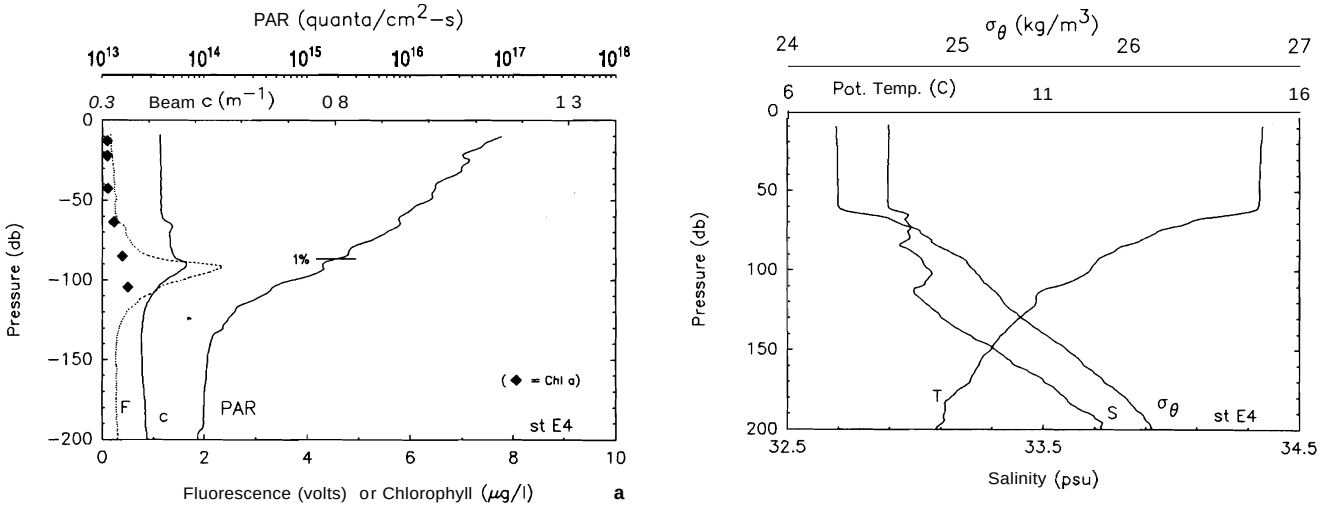

Fig. 2. (a) As in Figure 1*b*, but for station E4. (*b*) As in Figure 1*c*, but for station E4.

where above 190 dbar (Figure 1b). The measured 1% light level here is 31 dbar, and three distinct layers are found: (1) a near-surface layer above the 1% light level where chlorophyll concentrations are as high as 8.6 mg L^{-1}, (2) a deeper layer which extends from the 1% light level to about 110 dbar, and (3) a very deep layer with low beam *c* and and fluorescence levels which extends from 125 to 190 dbar. No surface mixed layer is observed, and gradients in all measured quantities extend to the surface. A weak temperature inversion is present on the upper boundary of layer 2 (Figure 1*c*) and suggests that this layer is intrusive, a conclusion also supported by the potential temperature-salinity (θ-S) diagram for this station. Examples of several θ-S diagrams showing an association between deep fluorescence layers and relatively warm, salty anomalies are given by Kadko et al. [this issue].

A very different type of profile is typically found in offshore waters away from the jet, such as at station E4 (Figure 1a). A deep fluorescence layer is centered at about 98 dbar, well below the 60-dbar deep surface mixed layer, and lies just below the 1% light level at 85 dbar (Figure 2*a* and 2*b*). Chlorophyll concentrations from bottle samples are about 0.5 mg L^{-1} just above and below the fluorescence peak; apparently the peak itself was missed in sampling. However, chlorophyll and fluorescence are highly correlated and nearby stations show peak concentrations of about 1 mg L^{-1}. Chlorophyll layers of this type, which occur in association with the base of the euphotic zone, are common features of the California Current system [cf. Anderson, 1969; *Cullen*, 1982]. They may result from a number of processes such as an increase in phytoplankton biomass due to growth at the intersection of the euphotic zone and nutricline [Herbland and Voituriez, 1979]. Two other possibilities are photoadaptation, where the chlorophyll per cell increases in response to low light conditions [Prezelin, 1981; Beers et al., 1975], or variability in fluorescence yield of the phytoplankton [Kiefer, 1973]. At station E4 and nearby stations the increase in beam *c* indicates increased biomass, while the fluorescence per unit chlorophyll, or fluorescence yield, is relatively constant throughout the water column. However, the chlorophyll per unit beam c increases with depth at E4 and suggests that the chlorophyll content per cell or per unit biomass also increases with depth.

To objectively examine CTZ data sets for the occurrence of phytoplankton layers which may have been moved out of the euphotic zone by subduction processes, it is necessary to differentiate the deep layers like those of Figure 1 from those which probably result from in situ photosynthesis as in Figure 2. Furthermore, it is necessary to rule out other processes which might also result in the presence of layers of fluorescent particles below the euphotic zone. A step in this process is to establish the relationship between the light field in the water column throughout the region and the vertical positions of layers of phytoplankton.

The penetration of light into the water column is examined by comparing vertical profiles of PAR throughout the CTZ. A total of 17 stations from legs 1 and 2 of the Thomas Washington survey, all recorded within one hour of local noon, are used to examine the variability of the light field (Figure 3*a*). Stations close to local noon were chosen in order to observe the maximum penetration of light into the water column. Following Huyer et al. [this issue], three regions are identified based on dynamic height (5/500 dbar): the jet corresponds to the range 0.82–0.96 m, inshore and southern waters below 0.82 m, and offshore and northern waters greater than 0.96 m. These ranges are somewhat different from those used by Huyer et al. [this issue] but are more appropriate to the Thomas Washington data. Considerable variation in the depth of light penetration is found within the jet waters: typical values of the 1% light level in the most turbid waters are in the range of 20 to 30 dbar and are almost 80 dbar in the more clear waters (Figure 3*b*). This depth range also spans that observed for the inshore and southern waters. Offshore waters are generally more clear, with a typical 1% light level of about 85 dbar; much of the phytoplankton in the water column lies below this level.

Observations obtained during leg 2 of the Thomas Washington survey show that almost one fourth of the water column with high chlorophyll fluorescence levels (>1.0 V) is found at depths below the 1% light level of the clearest offshore waters (Figure 3*c*). About 6.4% occurs below the 0.1% light level, which ranges from about 115 to 125 dbar on the basis of the three offshore profiles of Figure 3*b*. The threshold fluorescence value of 1.0 V is chosen because it represents a high signal level; the noise level of the fluorometer and CTD acquisition system used on the Thomas

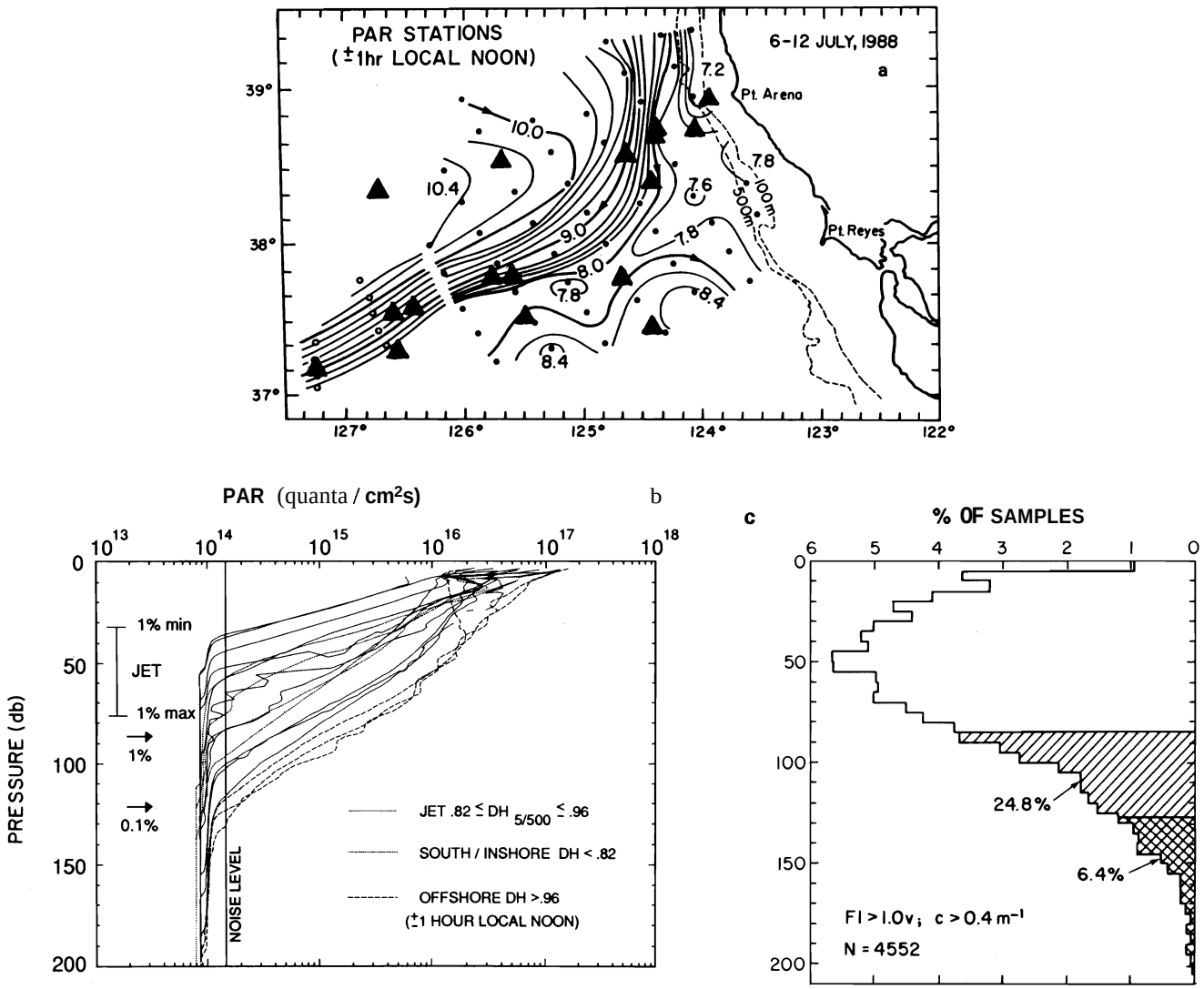

Fig. 3. (a) Location of PAR profiles obtained within 1 hour of local noon (triangles). Contours of geopotential anomaly (01500 dbar) are from the first Poinf *Sur.* survey, July 6–12, 1988. The offshore extension of geopotential anomaly contours is from leg 2 of the Thomas Washington survey. (*b*) PAR profiles obtained within 1 hour of local noon in the offshore jet (solid lines), southern and inshore waters (dotted lines), and offshore waters (dashed lines). The vertical bar shows range in 1% light level in jet. Arrows indicate depths of 1% and 0.1% light levels in clear offshore waters. (c) Histogram showing distribution of fluorescence in water column from all CTD profiles obtained during leg 2 of the Thomas Washington survey.

Washington is about a factor of 4 smaller. The tail of the distribution of Figure 3*c* extends down to 200 dbar, although layers exhibiting high fluorescence are found at depths exceeding 200 dbar in some of the other surveys. For stations within the jet, the fluorescence threshold used in producing the histogram of Figure 3*c* corresponds to a chlorophyll concentration of about 1 mg L^{-1} and in the offshore waters to a level of about 0.3 mg L^{-1}. The points sorted into the histogram also have beam c values exceeding 0.4 m^{-1}. Thus much of the phytoplankton lies below the euphotic zone.

4. Subduction Criteria

Because phytoplankton require light for growth and reproduction, it is unlikely that local production of particles by photosynthesis can account for particle layers below the euphotic zone. These correspond to the hatched regions of Figure 3*c*, particularly those below the 0.1% light level (cross-hatched region). This suggests that other processes are responsible for these deep layers, such as vertical circulation out of the euphotic zone, particle sinking, resuspension of bottom sediments containing chlorophyll, or diapycnal mixing. We have no microstructure measurements to assess diapycnal mixing rate and assume that this is not an important mechanism for vertical particle transport here.

The hypothesis that vertical circulation, or subduction, accounts for these layers has been investigated by *Kadko* et *al.* [this issue] and is supported by a variety of indicators. In addition to high levels of chlorophyll, these layers often contain deficiencies of ^{222}Rn ($\lambda_{1/2}$ = 3.85 days) with respect to ^{226}Ra activity, which indicates recent gas exchange with the atmosphere. The radon observations are perhaps the most unambiguous of all subduction indicators, since no other process can produce the deficiencies. The layers are

often associated with local maxima in dissolved oxygen and often appear in water masses which are warmer and saltier than waters above and below in θ-S diagrams. All of these observations are consistent with vertical movement of water masses away from the surface. However, a limitation of these indicators is that they are based on bottle sampling and therefore have very limited vertical resolution. Furthermore, the indicator ^{222}Rn is available for a relatively small number of stations and only as part of the *Thomas Washington* survey. In this analysis, we focus on the distributions of chlorophyll fluorescence and beam c as subduction indicators because they can be measured to about the same vertical resolution as CTD variables and because they are available from all surveys.

The possible role of particle sinking in forming the deep fluorescent layers is difficult to assess, although a number of factors suggest that it is not the dominant process. First, oceanic phytoplankton generally tend to sink slowly at vertical velocities of less than 1 m d^{-1} [*Bienfang,* 1981; *Bienfang and Szyper,* 1982; *Bienfang et al.* 1982; *Smayda,* 19701. Observations from the Point Conception area of California indicate that phytoplankton sinking rates within 50 km of the upwelling center are less than 2 m d^{-1} [*Bienfang,* 1985]. These estimates are much smaller than the vertical subduction velocity of 27 m d^{-1} obtained by *Kadko et al.* [this issue] based on ^{222}Rn samples.

Second, θ-S relationships observed in these deep layers found in offshore regions of the jet appear related to those found nearshore in the euphotic zone, as is shown later. If particle sinking were dominant, then the θ-S relationship of a layer would have no correspondence to properties in the euphotic zone from which the particles were derived. The θ-S of the layer would simply be the local relationship at the time and depth at which the particle layer is observed as it sinks downward. As an additional check on the possible role of particle sinking in forming the deep layers, the densities corresponding to layers nearshore in the jet were compared with those found offshore. No consistent increase is observed offshore as might be expected as a result of particle sinking over the time required to advect out the jet (a few days to a few weeks, depending on the position of a layer in the water column).

Third, many of the deep regions of phytoplankton are in thin, well defined layers which are more or less Gaussian in shape (e.g., Figure 6*f*). A distribution of descending particles all falling at different rates (but strongly weighted toward large numbers of small particles [cf. *Spinrad,* 1986]), for many days would tend to be spread vertically throughout the water column and would not concentrate in layers. Finally, in cross-axis sections of the jet, where the station spacing is about 10 km, distributions of fluorescence and beam c approximately parallel σ_θ surfaces. This would not be expected if particle sinking across density surfaces were dominant.

It is possible that particle sinking may work in combination with subduction processes in layer formation. In nearshore areas where chlorophyll concentrations are large, particle coagulation effects may be important [*Jackson,* 1991] and could result in much higher sinking rates, greater than 100 m d^{-1} [*Smetacek,* 1985]. However, the coagulated particles would have to have combined effective densities equal to the seawater density at some point in the water column to remain suspended. Otherwise, they would sink to the bottom.

Another possible mechanism which might result in fluorescent particles appearing below the euphotic zone is resuspension of bottom sediments containing phytoplankton. Deep nepheloid layers due to resuspension processes have been observed over the continental shelf off Oregon by *Pak and Zaneveld* [1977]. Turbidity layers with high values of beam c are commonly observed below 100 m in all of the CTZ hydrographic data sets, particularly nearshore. Typically these layers occur near the seafloor and exhibit no measurable fluorescence. However, deep turbidity layers from a few profiles exhibit very low, but measurable, fluorescence signals. Comparison of signal levels indicates that the ratio of fluorescence to beam c is much lower in these bottom resuspended layers than in the phytoplankton layers higher in the water column. These layers are easily differentiated because their θ-S relationships are very different from those found anywhere in the euphotic zone and the corresponding seawater densities are much greater. Another difference between the subducted layers and these deep turbidity layers is the ratio of phaeopigment to total pigment present. In the deep turbidity layers the ratio is often larger than 0.8 while in the subducted layers it is typically less than 0.4 (separate analysis by B. H. Jones).

On the basis of the preceding analysis, we conclude that the phytoplankton layers observed well below the euphotic zone, which exhibit high values and correlated distributions of fluorescence and beam c, result primarily from subduction processes. However, some clarification about "well below the euphotic zone" is required. The presence of phytoplankton below the 1% light level at a specific station does not necessarily mean that the phytoplankton were not produced in situ, because the depth of light penetration can change. For example, a layer of phytoplankton might initially grow near the deepest observed 1% light level of 80 to 90 dbar in clear water. After this growth, energetic near-surface advection could transport a second, more shallow layer of particles, over the deeper layer and produce a much shallower 1% light level. The result would be a deep layer of phytoplankton produced in situ which is observed below the euphotic zone. Other scenarios might also produce a similar situation. For this reason we generally limit our analysis to those layers found below the deepest 0.1% light levels which are found in clear, offshore waters. We have used a pressure of 120 dbar, about the midpoint of the range in 0.1% light levels in offshore waters (Figure 3*c*), to represent this point in the water column. While this is a very restrictive criterion, it does reduce the possibility that the observed particles result from in situ photosynthesis.

To objectively search each of the CTZ data sets for subducted water masses, we applied three criteria based on the preceding analysis. If all three of the following criteria are satisfied, we consider the water mass to have been subducted. The criteria are (1) pressure > 120 dbar, (2) beam $c > 0.4$ m $^{-1}$, and (3) fluorescence signal exceeding the instrumental noise level. For these data, a beam c threshold of 0.4 m $^{-1}$ or larger is found to differentiate turbid layers from more clear ambient waters. Minimum observed levels of beam c in individual profiles from all of the data sets fall in the range 0.35–0.40 m $^{-1}$ and are taken to be representative of the effective clear water values of beam c (c_c). This range of c_c falls within that given by *Baker and Lavelle*

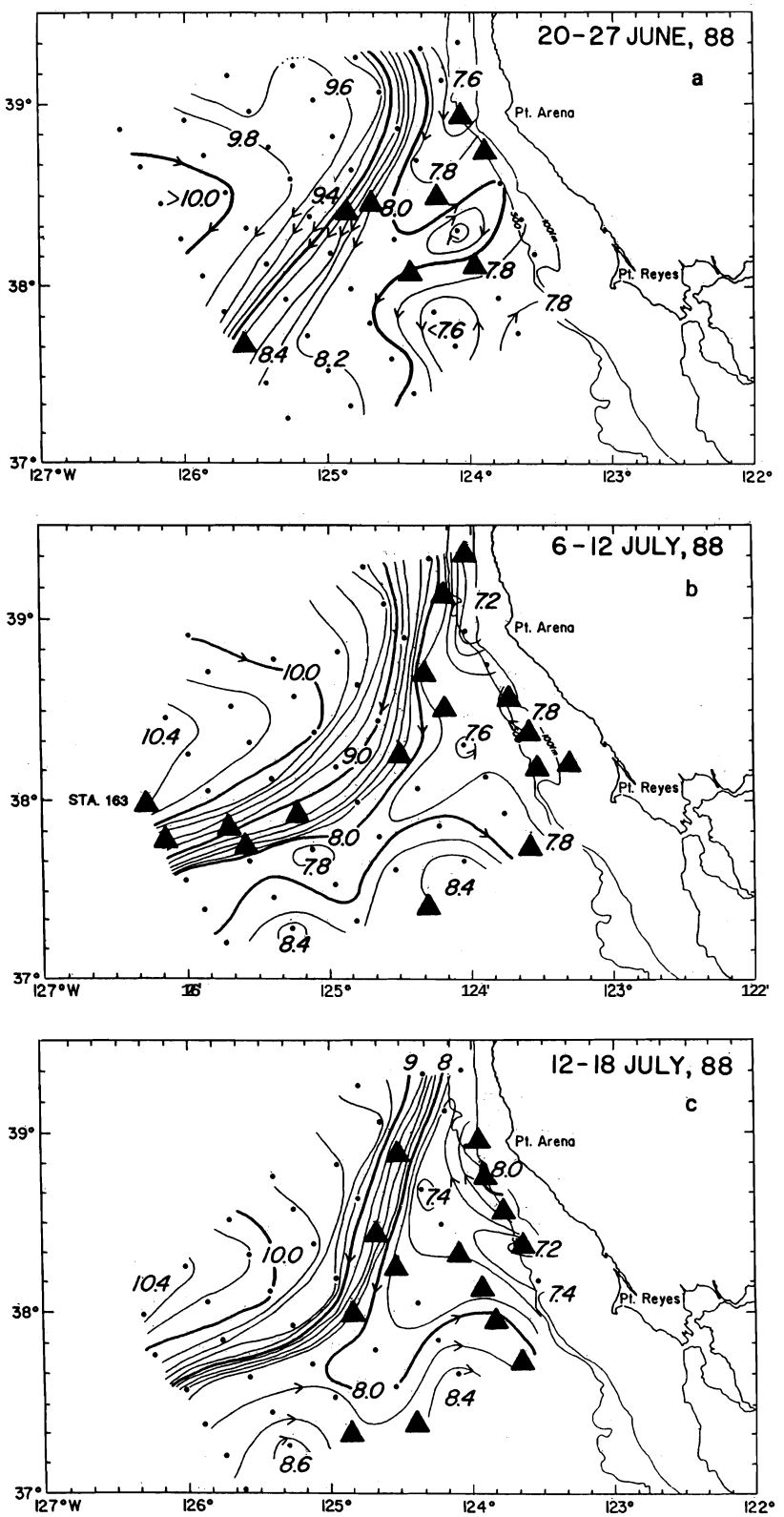

Fig. 4. Locations of stations containing subducted water masses, shown with solid triangles (dots show other station locations). (a) first Wecomo survey, July 20–27; (*b*) first *Point Sur.* survey, July 6–12; (*c*) second Point *Sur* survey, July 12–18; (*d*) third Point *Sur.* survey, July 21–27; and (e) second *Wecoma* survey, July 29 to August 4. Contours show geopotential anomaly (0/500 dbar).

[1984] of $0.31–0.42\ m^{-1}$. The range is also comparable to two experimental results for c_p presented by Jerlov [1976, Table XIII]: $0.319\ m^{-1}$ and $0.385\ m^{-1}$ (interpolated to 660 nm).

The threshold fluorescence signal level had to be determined individually for each of the surveys because the effective noise level for each fluorometer and CTD data acquisition system was different. The procedure for determining this threshold is basically subjective and is based on

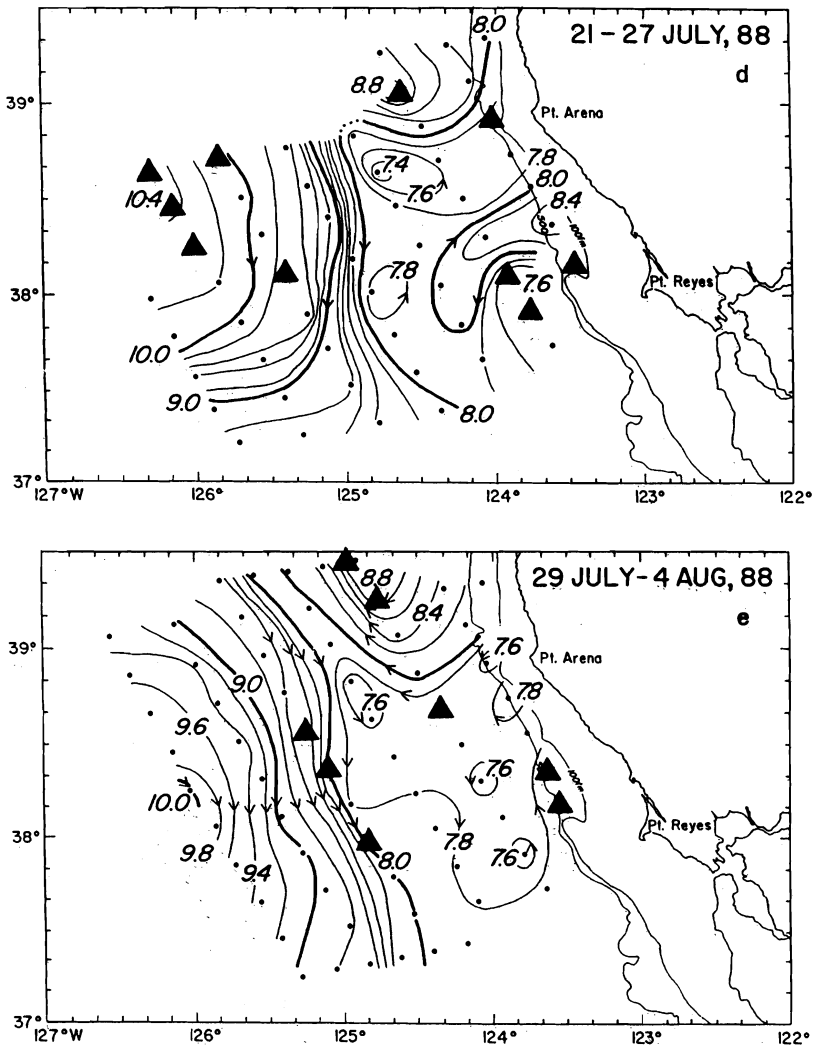

Fig. 4. (continued)

comparing signal levels in fluorescent layers with minimum observed levels which are taken to be the instrumental noise level. Minimum signal thresholds are derived from all of the survey data and are used in identifying subducted water masses. It proved impractical to use a uniform chlorophyll or total pigment concentration as a criterion for these data because of high scatter in the observed relationship between fluorescence voltage and pigment concentrations derived from bottle samples. Much of fhis scatter is apparently due to regional differences in the regression coefficients and may result from differences in phytoplankton species composition *[Hood,* 1990].

To search for subducted water masses, all of the CTZ data sets were sorted on the basis of the criteria developed above. Profiles from all surveys identified as containing subducted layers were individually examined to verify that noise spikes or other data problems were not present. This sorting procedure also identified a few layers near the seafloor with relatively high beam *c* but very weak fluorescence levels that barely exceeded the threshold. Water properties of these points are typical of the ambient deep water and they are usually found at depths exceeding 300 m. These points were excluded from the analysis.

5. Distribution of Subducted Water Masses

Subducted water masses occur frequently in the CTZ, given the number of profiles from each grid survey which contain them (Figure 4). They are found both in the seaward flowing jet and nearshore, and a few are found in offshore waters south of the jet. Beam c and fluorescence anomalies in the layers from these latter profiles were very weak, as were all of the layers in the first survey. In the first three surveys from June 20 to July 18, no layers are found in offshore waters to the north and east of the jet, and those farthest offshore during this time are in the jet itself. A different situation is observed during the fourth survey from July 21 to 27, when subducted layers are found near the offshore boundary of the grid. They are also seaward of the strongest flow in the jet. Over the time period from the third to fourth grid survey, the orientation of the jet rotated abruptly from offshore flow to alongshore flow, where it remained constant at least through the end of the fifth survey. The change in orientation coincided with a general relaxation in the wind field at this time (T. P. Stanton et al., Upper ocean response to a wind relaxation event in the coastal transition zone, submitted to *Journal of Geophysical*

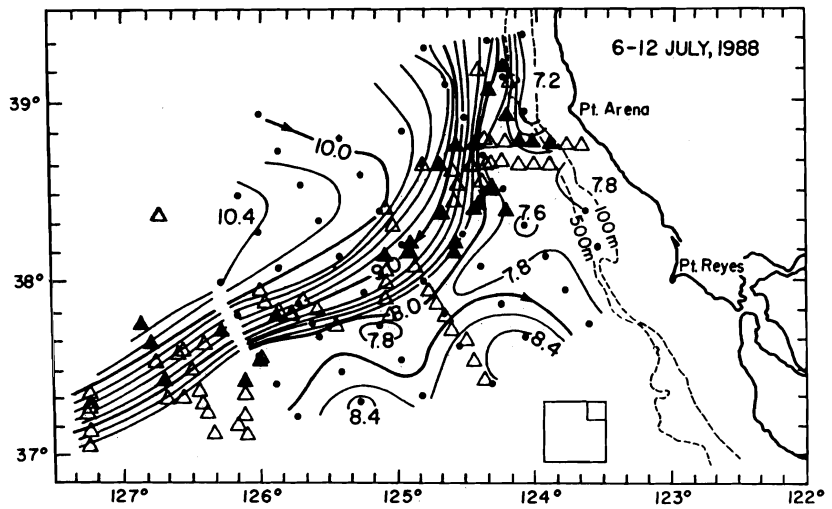

Fig. 5. Locations of all stations during leg 2 of the *Thomas Washington* survey (triangles). Solid triangles indicate stations with subducted water masses. Contours of geopotential anomaly (0/500 dbar) are from the first *Point* Sur survey, July 6–12, 1988. The offshore extension of geopotential anomaly contours is from the *Thomas Washington* survey. The large and small inset squares show the areas of a SO-m-deep euphotic zone that would be subducted by vertical volume fluxes of 80 and 5 $km^3\ d^{-1}$ (see section 8).

Research, 1990), a pattern which has been observed previously in the same area [*Strub* et al., this issue].

Leg 2 of the Thomas Washington survey was designed to sample selectively the seaward flowing jet and is therefore useful for examining the distribution of subducted water masses here. In addition, this survey included some stations outside of the jet for comparison. Application of the criteria developed in section 4 shows that subducted water masses are found frequently out along the jet axis with the most seaward of these stations lying almost 300 km from Point Arena (Figure 5). A few stations south of Point Arena and inshore of the jet are located in an anticyclonic eddy (M. Swenson et al., The dynamical and the thermodynamical structure of the flow associated with a cold filament off Point Arena, California, in July 1988, submitted to Journal of Geophysical Research, 1990, hereinafter referred to as Swensen et al., 1990) and also contain subducted water masses.

Profiles from a group of five stations from those identified in Figure 5 suggest a gradual sinking of phytoplankton layers along isopycnal surfaces out the jet axis (Figure 6*a*). These stations were not occupied sequentially and do not follow any particular water parcel in a Lagrangian sense. Rather, they illustrate where particle layers can be found in different regions of the jet. At the nearshore station 46, high levels of fluorescence and beam c are observed above 80 dbar. Radon deficiencies at this station indicate recent gas exchange throughout this depth range [Kadko et al., this issue] even though no surface mixed layer is present. Surface mixed layers in density are apparent only at offshore stations 67 and 33 in the upper 20 dbar. Out the axis of the jet, beam c, fluorescence, and chlorophyll levels are frequently high on and above the 25.8 isopycnal, which deepens from about 23 dbar at station 46 to 150 dbar at station 33. Discrete layers around this level are evident (Figures 6*c*, 6*e*, and 6f) but are not continuous in profiles from nearby stations. Measurable beam c and fluorescence levels are not limited to the depth of the 25.8 isopycnal and above, but exceed 200 dbar in some stations such as 17A (Figure 6*d*) and in stations from the five grid surveys of Figure 4 as well.

Figure 6 suggests that the vertical distribution of phytoplankton layers may be related to the position of isopycnal surfaces. Because of this we use an isopycnal coordinate system in much of the following analysis. In particular, the distributions of properties on two isopycnal surfaces are examined in some detail: (1) the 25.8, which frequently lies within the euphotic zone, and (2) the 26.2, which is generally below the euphotic zone.

Comparison of the distributions of beam c and pressure on isopycnal surfaces indicates that the lateral extent of subducted layers may be large. Offshore, where the 25.8 surface is below 120 dbar, beam c $> 0.4\ m^{-1}$ at stations 33, 34, 72, and 75 (Figures 7a and 7b); the along-axis separation of the 33-34 pair and the 72-75 pair is about 50 km while the cross-axis dimension of this layer of particles is at least 28 km. The pattern of isopycnal contours of fluorescence (not shown) is very similar to that for beam c in Figure 7*a*. The highest levels of beam c ($c > 0.7\ m^{-1}$) on the 25.8 isopycnal occur inshore where this surface lies within the euphotic zone (above 50 dbar based on Figure 3b) and is consistent with in situ production of phytoplankton. One of these areas where the 25.8 isopycnal is warped upward is centered on 124.25°W, 38.75°N, and results from the combination of the southward jet flow and the strong northward flow due to an anticyclonic eddy (Figure 11).

On the deeper 26.2 isopycnal the highest levels of beam c ($c > 0.5\ m^{-1}$) are found nearshore at depths below 120 dbar (Figures 8*a* and 8*b*), except for the area immediately south of Point Arena, which is very shallow and reaches above 50 dbar. Farther offshore and west of 125.5°W, all points having c $> 0.4\ m^{-1}$ lie below 120 dbar. Again, the pattern of fluorescence on this surface (not shown) is very similar. We conclude from this that most of the phytoplankton found on the 26.2 isopycnal in the area covered by the survey were not produced in situ where observed but instead have been moved vertically and horizontally by subduction and advection processes out of the euphotic zone in their source regions. This suggests that subduction processes play an important role in governing water mass properties on this

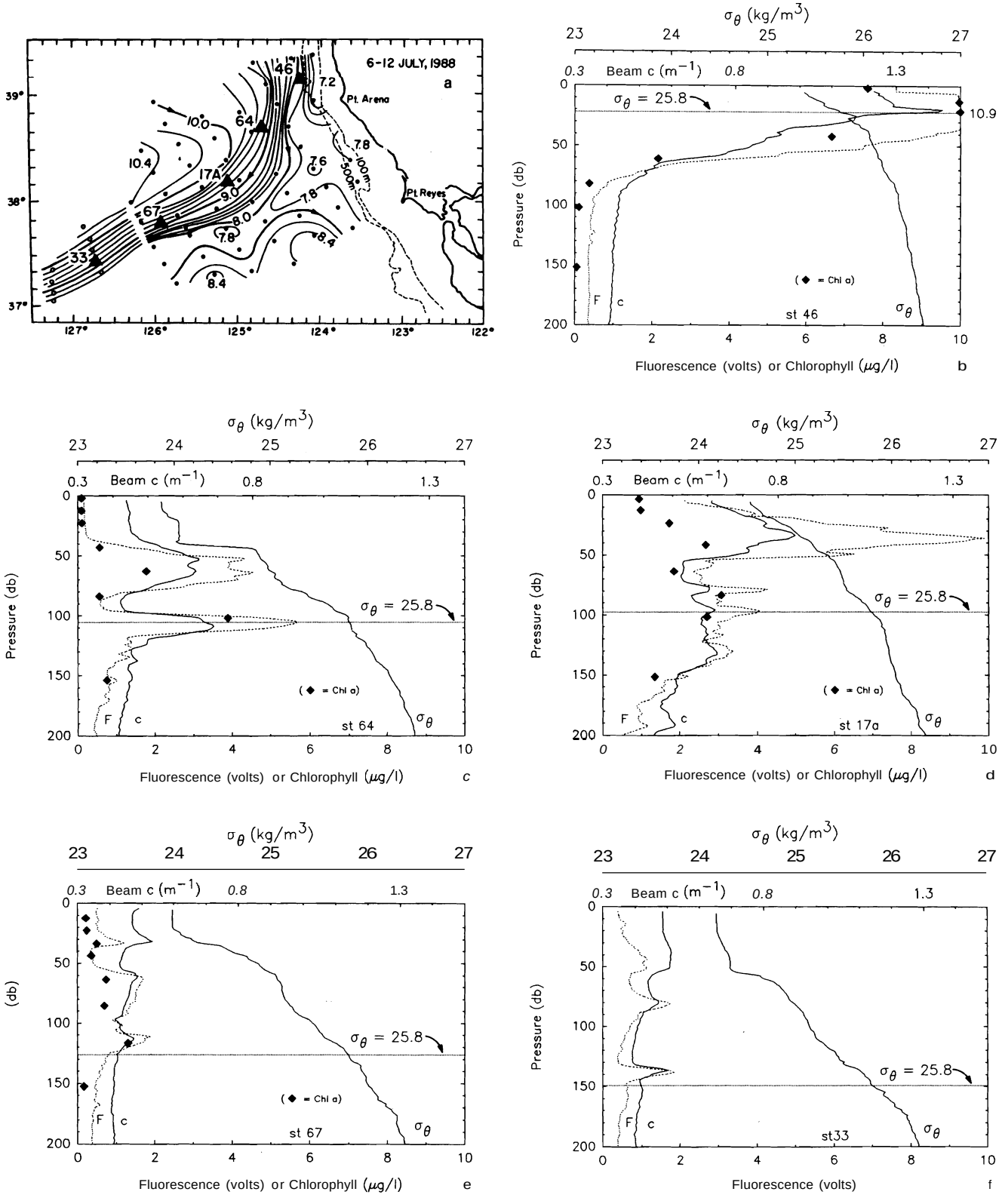

Fig. 6. (a) Locations of stations 46, 64, 17A, 67, and 33 along the jet axis, and profiles of potential density, beam c, and fluorescence at stations (*b*) 46, (c) 64, (*d*) 17A, (*e*) 67, and (*f*) 33. Diamonds indicate chlorophyll concentrations from bottle samples.

isopycnal surface. In contrast, in situ production within the survey area may account for much of the phytoplankton on the 25.8 surface nearshore, with subduction processes being more important offshore.

6. Sources of Subducted Water Masses

The distribution of beam *c* and fluorescence on isopycnals like the 26.2 indicate that many of the deep phytoplankton

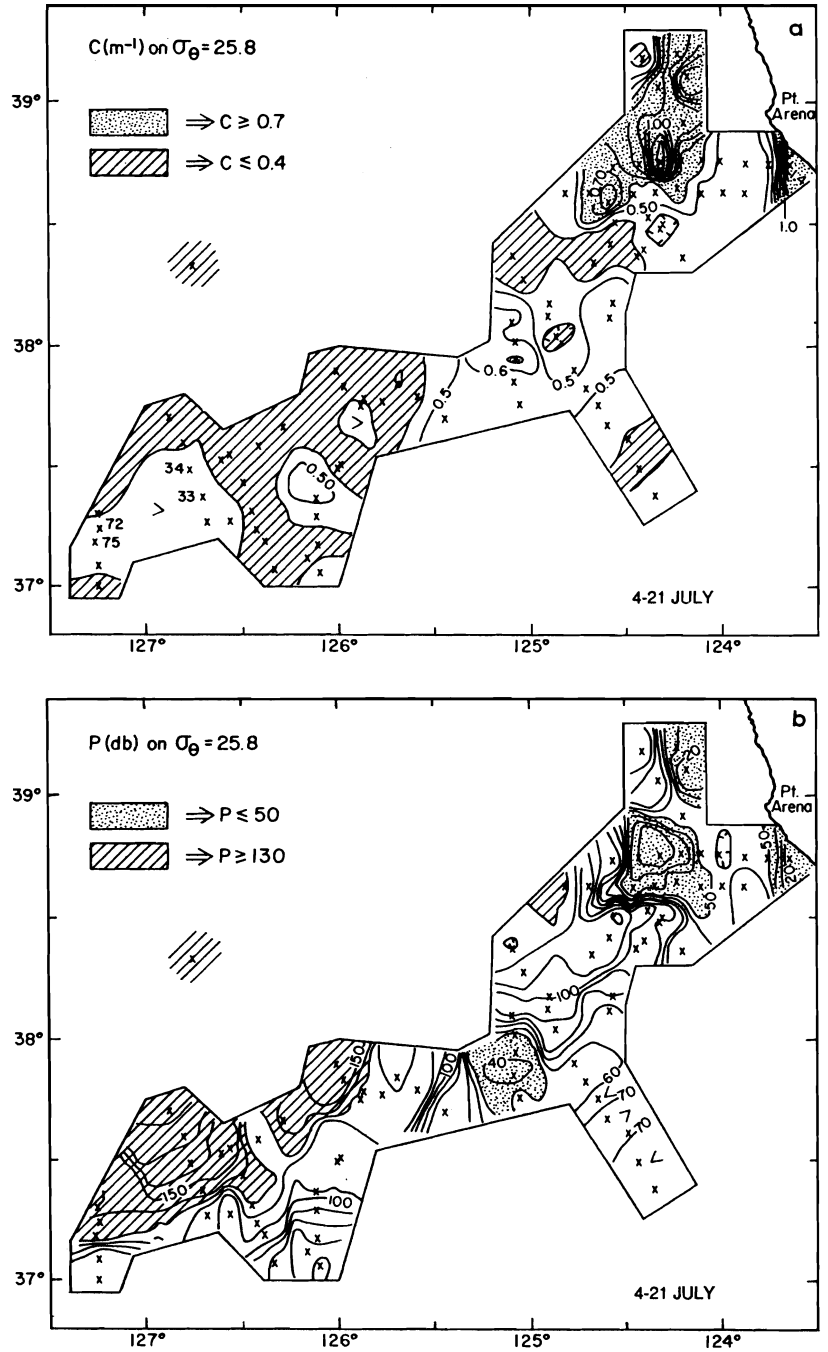

Fig. 7. Contour sections of *(a)* beam c and *(b)* pressure on $\sigma_\theta = 25.8$. The crosses show station locations.

layers probably originate in the euphotic zone away from where they are observed. Because isopycnals slope steeply upward toward the coast in the CTZ area, some lie within the euphotic zone nearshore but at much greater depths farther offshore (Figures 7*b* and 8*b*). We hypothesize that these inshore areas where the isopycnals rise into the euphotic zone are the major source regions for the phytoplankton and subducted water masses, although some sources probably lie to the north of the area covered by the surveys. Use of the term "source region" for subducted water masses simply means that they were near the surface there.

If the deep phytoplankton layers originate near shore, then the θ-S relationships in the layers found offshore should be similar to those nearshore in the euphotic zone if isopycnal and diapycnal mixing rates are not too large and if particle sinking is not important. For purposes of tracing vertical water mass movement, the phytoplankton act as a dye identifying water masses that have previously been in the euphotic zone. The 0-S characteristics are potentially useful for tracing horizontal movement of these water masses if remote source regions can be unambiguously identified in θ and S. In contrast to θ and S, which are conservative away from the mixed layer, beam c and fluorescence levels are likely to change substantially since phytoplankton concentrations are nonconservative over time scales of a few days and levels change as a result of a variety of processes such as

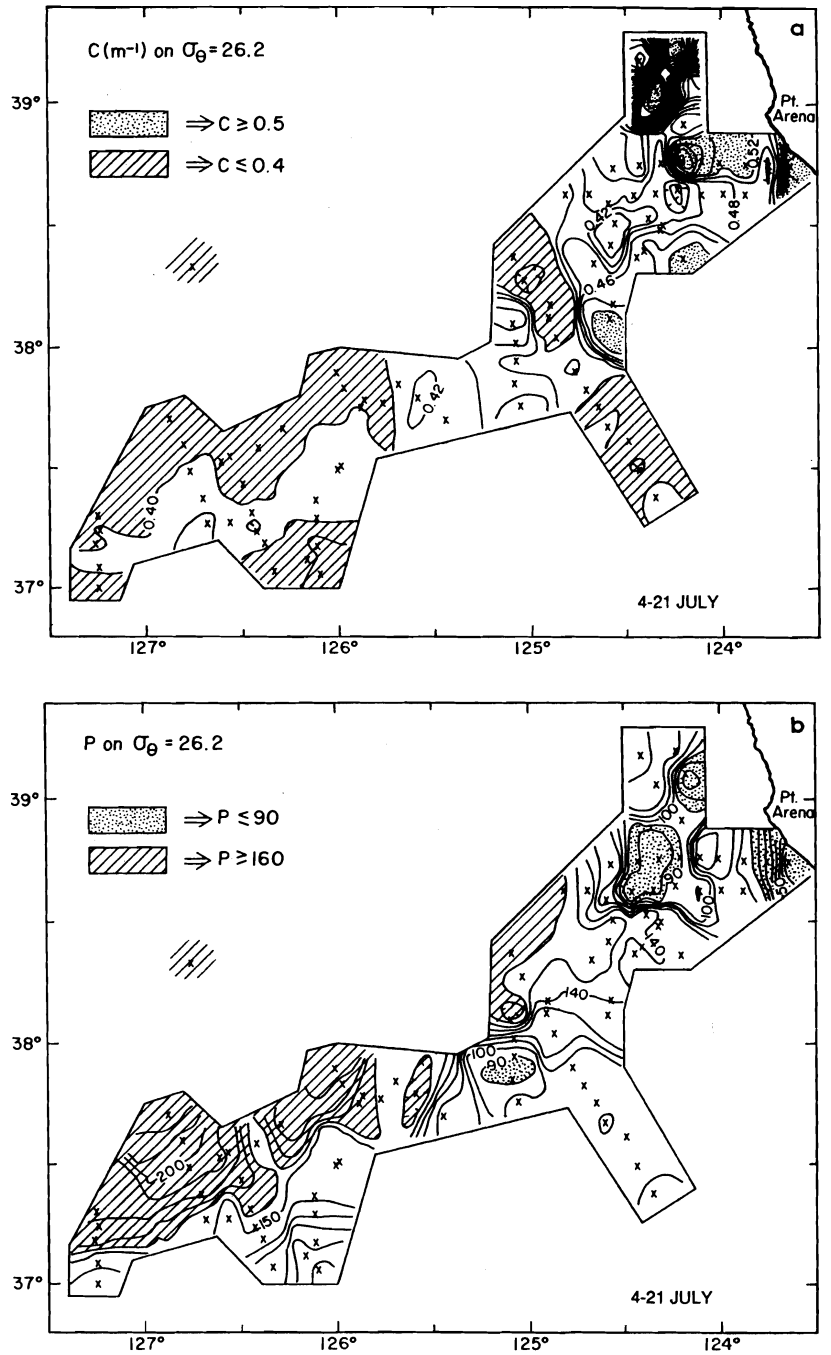

Fig. 8. Contour sections of (a) beam *c* and (*b*) pressure on $\sigma_\theta = 26.2$. The crosses show station locations.

photosynthesis and grazing by zooplankton. Therefore the usefulness of fluorescence and beam c as vertical water mass tracers will be limited by their effective loss rates.

In the remainder of this section, the θ-S characteristics of subducted water masses are compared with those of potential source regions for two (overlapping) time periods: first, over the entire experimental period, including the time when the jet orientation changed rapidly (late July to early August), and second, during the time when the jet orientation was fairly stable (late June to mid-July). Higher resolution sampling from the ***Thomas Washington*** during this latter period allows more detailed inferences to be drawn regarding near shore source regions.

The loci of all **0-S** points from the five grid surveys of Figure 4 which satisfy the subduction criteria of section 4 cluster into two areas of distinct characteristics (Figure **9*a***). Most of the points fall within a σ_θ range of **25.9–26.6** (group A), while a second group is clustered between **25.1** and **25.5** (group B). Most of the points in the second group are found at the offshore stations in Figure 4d (from the third ***Point Sur*** survey) when the jet orientation changed abruptly. The one exception is offshore station **163** (Figure **4*b***) from the first ***Point Sur*** survey, which also falls in Group B. The differences in θ-S characteristics of group B suggest that the subducted layers found offshore, particularly after the jet reorientation, are not derived from the same sources as those found elsewhere.

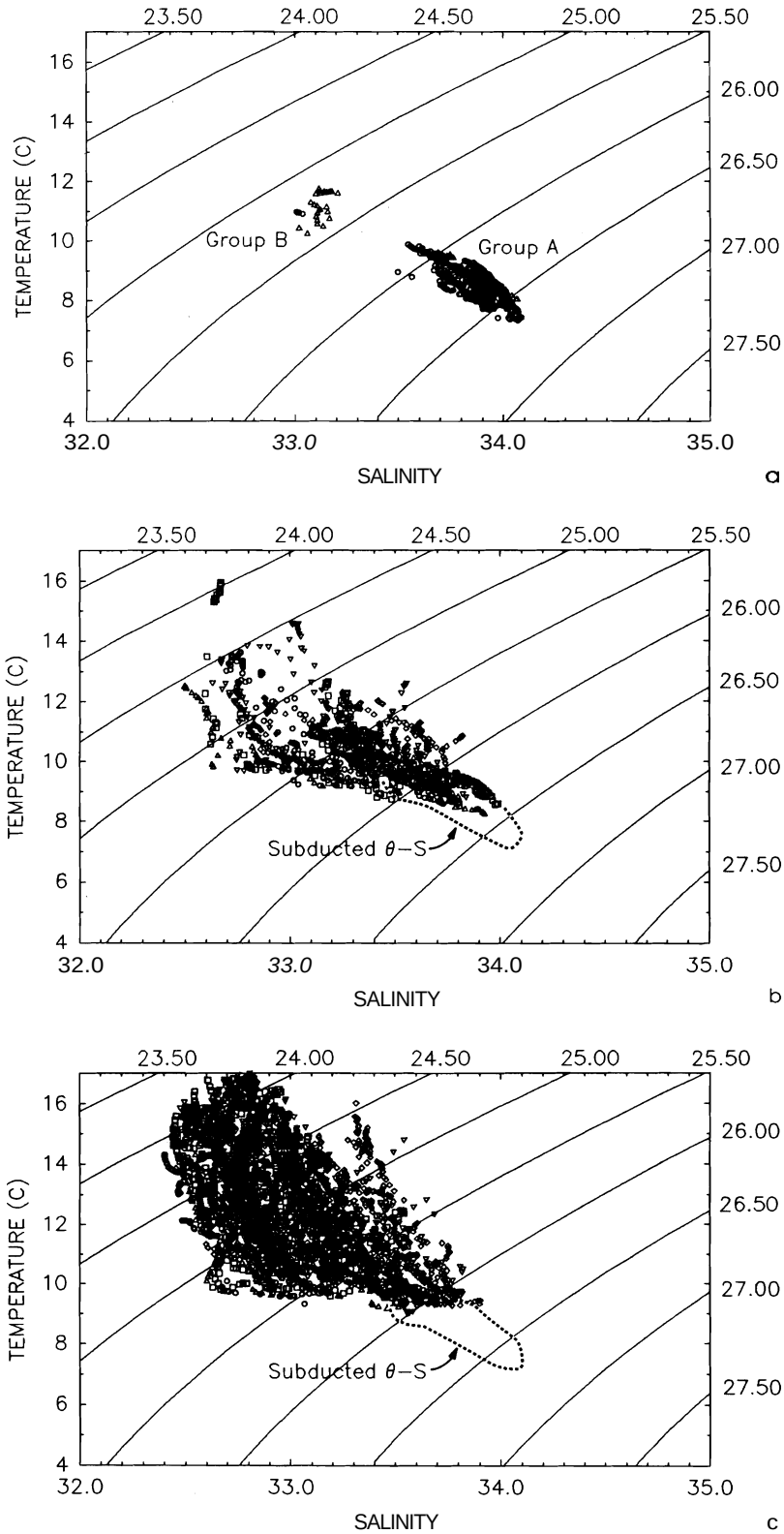

Fig. 9. (a) Plot of θ-S points corresponding to subducted water masses from the five grid surveys of Figure 4. Water masses of points in group A are from nearshore sources, and those of group B are from offshore sources. (b) Plot of θ-S points in the upper 50 dbar of the water column for the most inshore line of the five grid surveys of Figure 4. The envelope of θ-S points of subducted water masses in group A (Figure 9*a*) is shown by dashed lines. (*c*) Plot of θ-S points in the upper 50 dbar of water column for the offshore lines of the five grid surveys. The envelope of θ-S points of subducted water masses (Figure 9*a*) is shown by dashed lines.

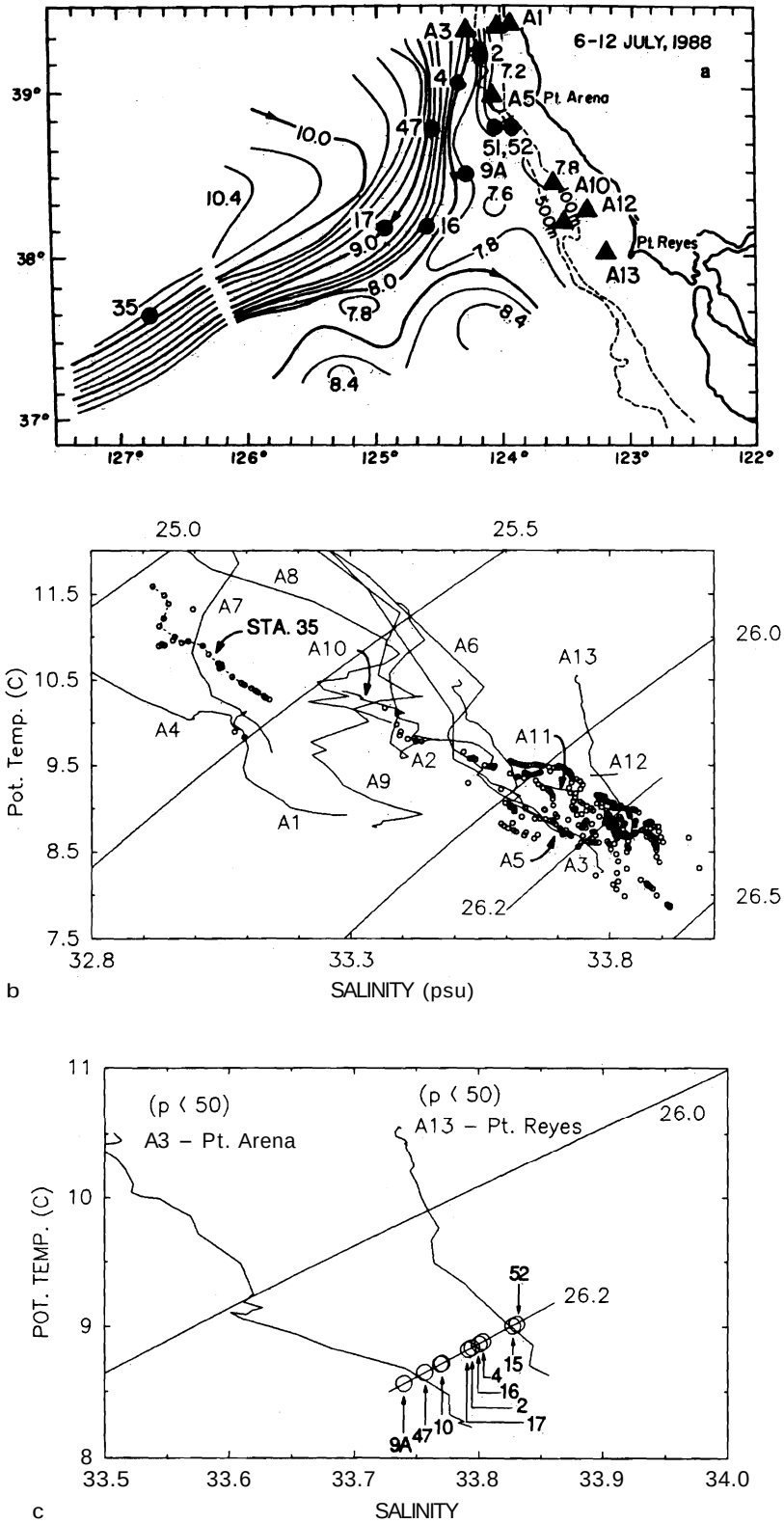

Fig. 10. (a) Locations of various stations whose θ-S relationships are shown in Figures 10*b* and 10*c*. (*b*) Plot of θ-S profiles (shown with solid lines) for the stations on line A from leg 1 of the Thomas Washington survey, and of θ-S points (shown with open circles) for subducted water masses observed below 120 dbar from leg 2 of the Thomas Washington survey. (*c*) Plot of θ-S points of subducted water masses on $\sigma_\theta = 26.2$ and θ-S profiles for the upper 50 dbar of the water column at stations A3 and A13 (solid lines).

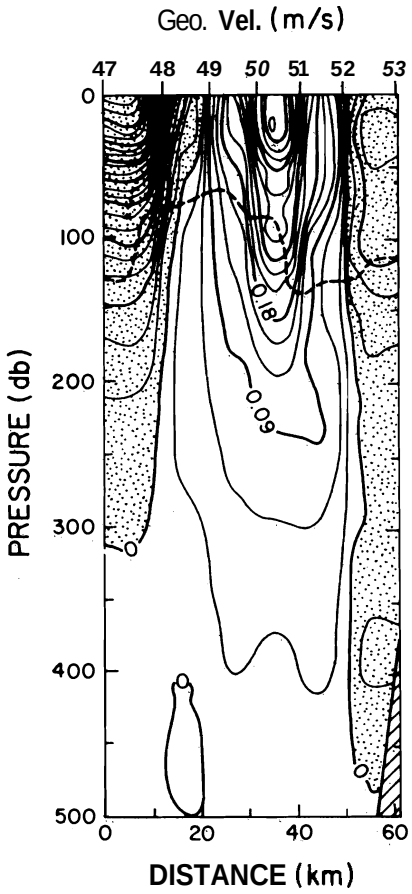

Fig. 11. Vertical section of geostrophic velocity (51500 dbar) computed from stations 47–53. Station locations are shown in Figure 14a. Stippled areas indicate flow to the south. The dashed line shows the position of $\sigma_\theta = 26.2$.

Subducted water masses corresponding to the main group of points (group A) in Figure 9*a* are probably derived from nearshore sources on the basis of comparisons with upper ocean ***θ-S*** characteristics in the CTZ area. All ***θ-S*** points in the upper 50 dbar of the water column from each inshore line of the gird surveys are plotted in Figure 9b along with the envelope of points from the subducted layers shown in Figure 9*a* (group A). The extensive overlap of the group A ***θ-S*** points with points from the inshore lines is consistent with nearshore source regions for the subducted water masses. In contrast, very little overlap is found between the group A subducted layer ***θ-S*** points and those from all of the other (offshore) lines from the grid surveys (Figure 9*c*). The upper 50 dbar of the water column is chosen because this range falls within the euphotic zone throughout most of the survey area (Figure 3b). However, this may underestimate the depth range of the euphotic zone in oearshore areas, since some of the θ-S points in the subducted layers correspond to higher densities than found near shore above 50 dbar.

It is also likely the majority of the subducted water masses observed within the jet during the process of sampling from the Thomas Washington (Figure 5) result from nearshore sources. During this sampling, the position and water mass composition of the jet were fairly constant for about a month covering the period June 20 to July 18 [Huyer et al., this issue]. The consistent orientation of the jet may be seen in the first three geopotential anomaly fields of Figure 4. Most of the ***θ-S*** points within the subducted layers of the jet, identified in Figure 5, fall within the group A envelope of ***θ-S*** points in Figure 9*a*. However, a few such as those from station 35, which is located far offshore, fall within the group B envelope and may indicate another source farther offshore (Figures 10*a* and 10*b*).

The ***θ-S*** points for the subducted water masses within the jet are consistent with formation by isopycnal mixing of waters from different near shore source regions. On the basis of ***θ-S*** distributions in the upper 50 dbar of the water column, two potential source regions are identified: (1) the waters offshore and north of Point Arena (and possible north of the study area), represented by station A3, and (2) waters immediately north of Point Reyes, represented by station A13 (Figure 10*b*). Points lying between the A3 and A13 curves could be formed by advection and isopycnal mixing of waters from these two source regions. However, source water contributions from the area around Point Reyes require a northward coastal flow inshore of the jet. The ***θ-S*** curves of Figure 10*b* (solid lines) are obtained from leg 1 data of the Thomas Washington survey (June 25 to July 2) and show that waters on the southern end of the inshore line are generally saltier on a given isopycnal than those to the north. This situation persisted during all of the grid surveys based on isopycnal plots of "spiciness" presented by Huyer et al. [this issue].

On some isopycnals near shore, a correspondence is observed between flow direction and ***θ-S*** properties which is consistent with the hypothesis that the subducted layers originate from at least two inshore source regions. A detailed ***θ-S*** diagram containing only points in subducted water masses below 120 dbar, which lie on $\sigma_\theta = 26.2$ (Figure 10*c*) shows that ***θ-S*** points at stations 9A and 47, in the southward flow of the jet (Figure 10*a*), are very similar to those at station A3 located north of Point Arena. The southward flow of the jet at station 47 penetrates to about 300 dbar and the maximum near-surface geostrophic velocity is 0.7 m s^{-1} (Figure 11). Contours of geostrophic velocity (reference level of 500 dbar) of Figure 11 are based on a line of stations extending offshore from just south of Point Arena (stations 47–53 in Figure 14*a*). In contrast, at stations 51 and 52, which are in northward flow (Figure 11), ***θ-S*** points are nearly identical to those at station A13 located just off Point Reyes. The remaining points lie between these end-members. The combination of northward flow in the center of the line of stations 47–53 with southward flow on the east end of the line (Figure 11) is due the presence of the anticyclonic eddy just inshore of the jet mentioned previously. This eddy is evident in drifter tracks reported by Swenson et al. (1990). A similar pattern of geostrophic velocity is also observed 20 km to the south on the line of stations 57-65 (station locations are shown in Figure 14*a*).

Further evidence that Point Reyes may be a source region for some of the subducted layers is the distribution of S on $\sigma_\theta = 26.2$ from legs 1 and 2 of the Thomas Washington survey. Salinities exceeding 33.82 are found on the two lines of stations from leg 2 that extend offshore from just south of Point Arena (Figure 12); these points generally are found below 90 dbar (Figure 8*b*) and have high levels of beam c (Figure 8*a*) and fluorescence. Two of these stations, 51 and 52, satisfy the subduction criteria of section 4. The high salinity of these waters ($S > 33.82$) is consistent with

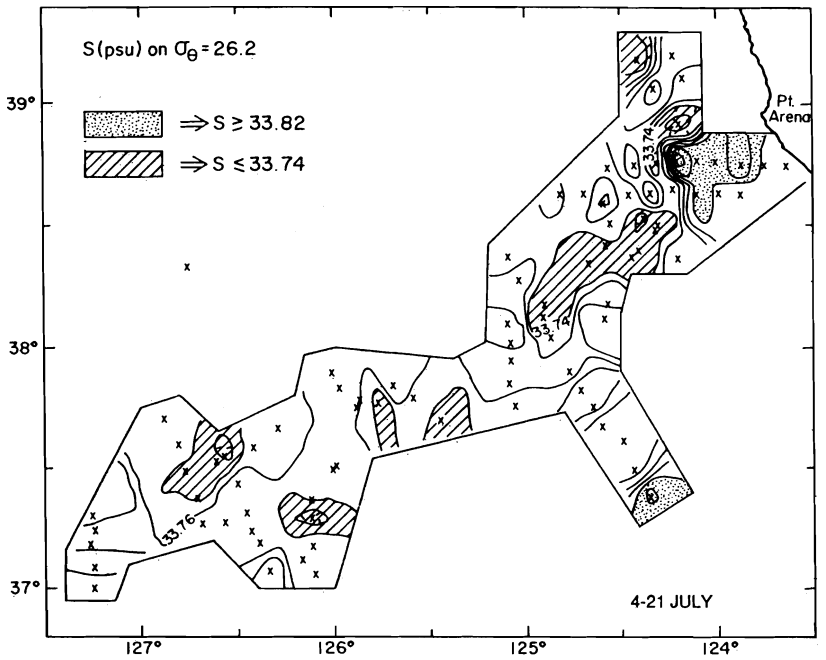

Fig. 12. Horizontal contour section of salinity on $\sigma_\theta = 26.2$ from leg 2 of *Thomas Washington* survey from July 4–21. Station locations are indicated with crosses.

northward (and downward) advection from the Point Reyes area along the 26.2 isopycnal. The more comprehensive inshore survey (leg 1) obtained about 18 days earlier shows that $S > 33.82$ on $\sigma_\theta = 26.2$ at three stations (A11, A12, and A13) near Point Reyes but nowhere to the north (Figure 13*a*). Clearly, considerable evolution of the nearshore salinity field occurred over this time period. Northwestward advection of high-salinity water along $\sigma_\theta = 26.2$ from the vicinity of Point Reyes would require an average speed of about 0.07 m s^{-1} to account for the changes in S near Point Arena. This estimate falls well within the range of northward geostrophic velocities on the 26.2 isopycnal along the line of stations 47–53 (Figure 11).

Not only is the salinity distribution consistent with the idea that Point Reyes is a subduction source region, but so are the distributions of beam c, fluorescence, and pressure on $\sigma_\theta = 25.2$. In the waters off Point Reyes, the 26.2 isopycnal reaches vertically to within about 40 dbar of the surface (i.e., within the euphotic zone) at station A13 (Figure 136) and has $c > 0.8$ m^{-1} (Figure 13*c*). High levels of beam c at pressures of about 90 dbar and less are evident at stations A11, A12, and A13. The fluorescence contours (not shown) are very similar to the beam c contours here. Thus waters found near Point Arena below 120 dbar, such as at stations 51 and 52, may originate in the near the surface waters off Point Reyes where similar S, beam c, and fluorescence characteristics are found.

7. Vertical Transport by Isopycnal Sinking

One mechanism that could result in vertical movement of water masses out of the euphotic zone and subsequent transport offshore to depths exceeding 120 dbar is simply flow along sloping isopycnal surfaces out the axis of the jet. Evidence for water mass sinking in the jet comes from a sequence of CTD stations made daily alongside a surface drifter (path shown with solid line in Figure 14*a*). Averages of densities in the upper 10 m of the water column progressively decrease, and the total change from the beginning to the end of the track is about 0.7 kg m^{-3}. Fluid particles traveling on the 25.8 or 26.2 isopycnal surfaces could experience depth changes of well over 100 m based on the distributions of pressure of these surfaces (Figures 76 and 8*b*). A particle moving on a density surface would probably not change depth monotonically because local depth variations result from processes like mesoscale eddy activity.

The time required for a water particle to move out the jet axis on a particular isopycnal varies greatly because of strong vertical shear in the jet. Depending upon the mean advective speed and the depth of a particular isopycnal, the time scale for this process to occur ranges from a few days to a few weeks. This advective time scale is of interest because it puts a lower bound on the persistence time for the subduction indicators used in this analysis (beam c and fluorescence) and it gives an estimate of the order of magnitude of typical vertical velocities. To illustrate how this isopycnal sinking out of the euphotic zone might proceed, the advection times and vertical and horizontal velocities are computed along hypothetical drifter tracks located on the 25.8 and 26.2 isopycnal surfaces.

Advective time scales for flow along these isopycnals are estimated from eight sections of geostrophic velocity which cross the jet at approximately right angles to the flow (Figure 14*a*). The sections were obtained over a 2-week period (July 7–21) during the time when the position of the jet was relatively constant [*Huyer et al.*, this issue]. Geostrophic velocity profiles are computed from adjacent pairs of stations on these transects and use a reference level of 500 dbar. Some sections show sloping density surfaces down to 500 dbar, so actual velocities may be larger. Geostrophic velocities are then interpolated onto the isopycnals based on the average pressure of the given isopycnal for each pair of stations; examples of isopycnal velocity profiles on $\sigma_\theta =$

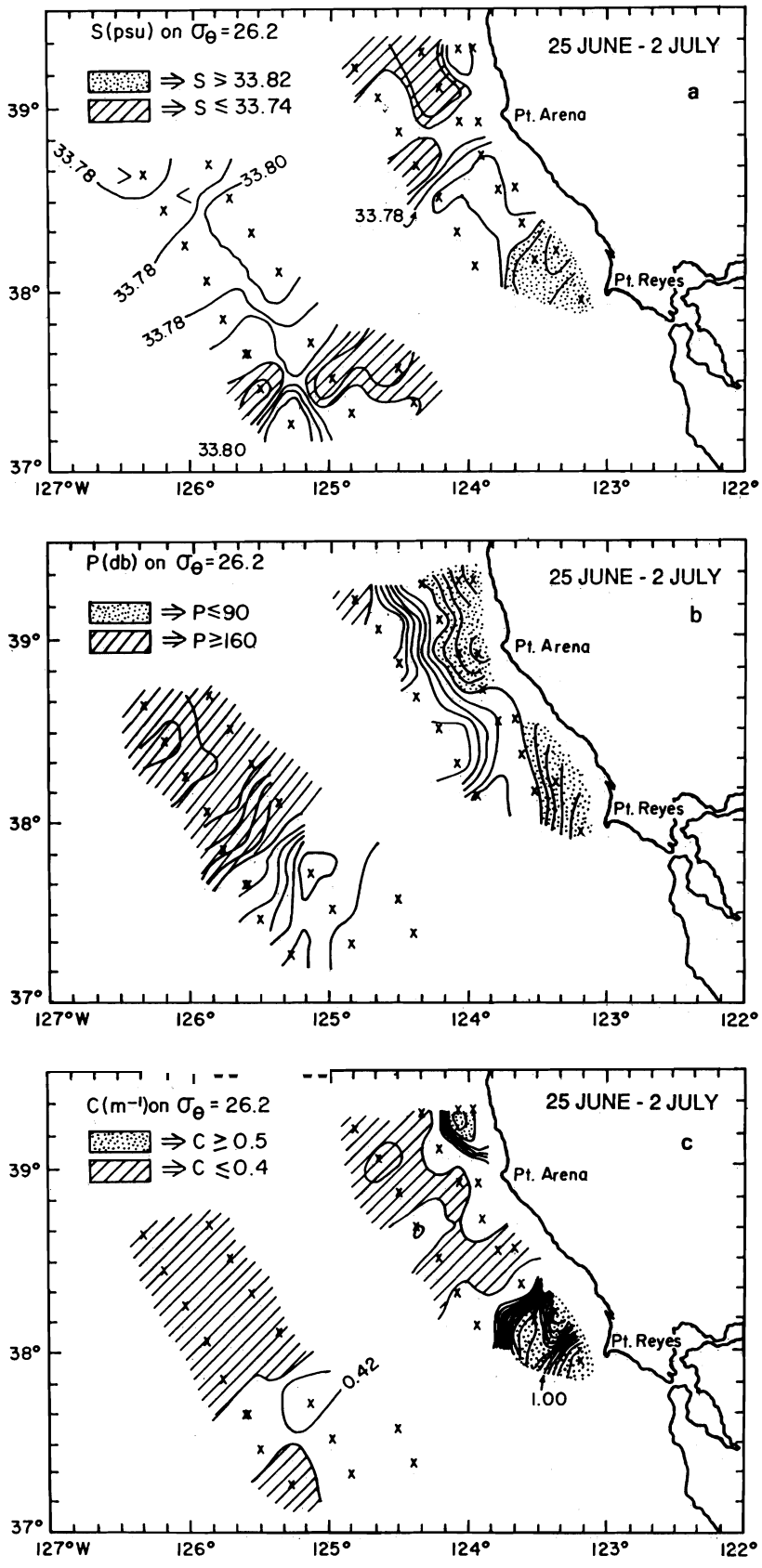

Fig. 13 Horizontal contour sections on σ_θ = 26.2 from leg 1 of *Thomas Washington* survey of *(a)* salinity, *(b)* pressure, and *(c)* beam c. Station locations are indicated with crosses.

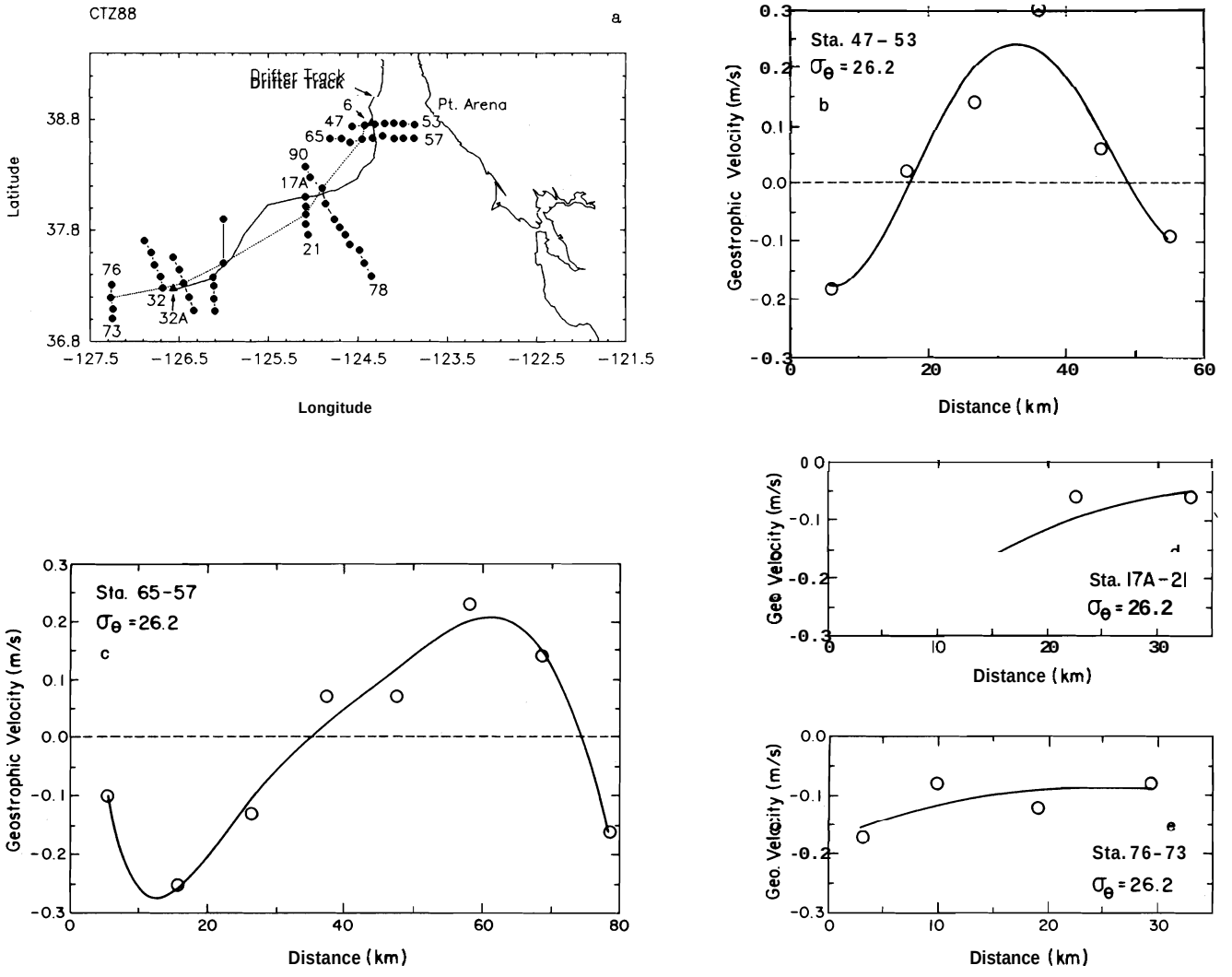

Fig. 14. (*a*) Cross-jet transects used for computing sections of geostrophic velocity (the surface drifter track is shown by the solid line and the hypothetical drifter track by the dotted line), and the isopycnal profiles of geostrophic velocity on $\sigma_\theta = 26.2$ for (*b*) stations 47–53, (*c*) stations 65–57, (*d*) stations 17A–21, and (e) stations 76–73.

26.2 are shown in Figures ***14b*** to ***14e.*** Negative velocities indicate generally southward or offshore flow, and the shapes of the profiles are approximated by polynomial fits to data points from station pairs.

On the two inshore lines ***47–53*** and ***65–57,*** a region of strong cyclonic vorticity separates the southward flowing jet from the northward flow of the anticyclonic eddy (Figure 14*b* and 14*c*). The region of southward flow in the eddy is barely resolved on the east end of each line. Farther out the jet along the line of stations ***17A*** to 21, the flow field exhibits lower vorticity and is offshore everywhere in the profile (Figure 14*d*). The mean velocity from this profile is -0.14 m s^{-1}. The offshore flow of the jet is still detectable at the most offshore line ***73–76, 360*** km from shore, and shows lower vorticity with a mean velocity of -0.11 m s^{-1}.

Advective time and velocity scales along the hypothetical drifter tracks at three levels in the jet are summarized in Table *1.* Mean velocity and time scales are based on averages of only the portions of each profile which are in the jet (southward or offshore flow); eddy or recirculating portions of isopycnal velocity profiles are not included in the means. The minimum time scales and maximum velocity scales are

TABLE I. Advection Times and Velocities Along Jet

	Time, days		Horizontal Velocity, m s^{-1}		Vertical Velocity, m s^{-1}	
Level	Minimum	Mean	Maximum	Mean	Maximum	Mean
5 dbar	5	11	0.70	0.33		
$\sigma_\theta = 25.8$	12	21	0.30	0.17	10	6
$\sigma_\theta = 26.2$	20	42	0.18	0.09	4	2

Stations (out axis of jet) are 48, 62, 88, 19, 26, 39, 32, and 75. Total distance is 321 km.

based on the maximum jet velocity in each section. We take minimum transit times and maximum velocities to be more representative of the jet axis, while the mean times and mean velocities are representative of off-axis conditions. The end points for the hypothetical drifter tracks are stations 48 and 75, and the track length is 321 km (dotted line, Figure 14*a*). The hypothetical drifter on the 25.8 isopycnal begins at about 20 dbar at station 48, well within the euphotic zone, and requires from 12 to 21 days to reach station 75, where it would be at about 140 dbar. The corresponding times on the 26.2 surface are about double these times, while those at 5 dbar are about half. For comparison, the track of an actual surface drifter is also shown in Figure 14 (solid line). This drifter took 5.1 days to travel from station 6 to station 32A, which compares favorably with minimum and mean times (between stations 48 and 32A) of 4.5–9.8 days using the geostrophic velocities at 5 dbar/500 dbar in the cross-jet sections of Figure 14*a*.

8. Discussion and Conclusions

Shipboard CTD and bio-optical observations made during the summer upwelling season in 1988 reveal the presence of deep phytoplankton layers below the euphotic zone in many areas of the coastal transition zone (CTZ), including a strong baroclinic jet which was present throughout the observational period. A principal conclusion of this study is that the water masses associated with the phytoplankton have been moved downward by subduction processes. This finding is supported by the distributions of several hydrographic and geochemical tracers, including ^{222}Rn, chlorophyll, and dissolved oxygen [Kadko et *al.*, this issue]. Criteria to objectively identify subducted water masses have been developed and are based on the light field in the water column and levels of chlorophyll fluorescence and the beam attenuation coefficient (beam c). Subducted water masses are observed in all six hydrographic grid surveys of the CTZ experiment, which covered the period June 20 to August 4, 1988.

The θ-S relationships corresponding to the subducted water masses fall into two distinct groups and are consistent with two near-surface subduction regions, one nearshore and a second much farther offshore. The scatter in θ-S points suggests that the nearshore source is distributed alongshore and has contributions from the area in the vicinity of Point Reyes and from an area north of Point Arena, or possibly north of the study area. Subducted water masses from the nearshore region were present throughout the experimental period, while those from the offshore source were most frequently observed just after the strong baroclinic jet changed orientation from offshore to alongshore flow.

The positions of layers of phytoplankton in the water column indicate that some water masses sink over 100 m as they are advected out along the jet axis. Similar, but much larger, vertical displacements resulting from isopycnal advection in a strong, meandering baroclinic jet (the Gulf Stream) have been observed in RAFOS float trajectories by Bower and Rossby [1989]. Vertical displacements could also result from mixing processes acting along sloping isopycnals, both along and across the jet axis. Vertical advection rates based on geostrophic flow on sloping density surfaces are 6–10 m d^{-1} for the 25.8 surface and 2–4 m d^{-1} for the deeper 26.2 surface. These estimates are averages based on advection over 320 km of the jet axis and probably underestimate maximum vertical velocities. This is because isopycnals rise up into higher-velocity flow nearshore where isopycnal slopes are generally the largest. Kadko et al. [this issue] estimate vertical velocities as high as 27 m d^{-1} based on ^{222}Rn deficiencies. Advective time time scales out the jet are about 2–3 weeks along the 25.8 isopycnal and about double this along the 26.2 isopycnal. This indicates that detectable levels of beam c and fluorescence from subducted phytoplankton can persist for several weeks.

A variety of other physical processes may lead to water mass subduction, and not all of them are associated with the jet, since subducted layers are found at several stations outside of the jet (Figures 5 and 6). Drifter observations of Brink et al. [this issue] show that convergence zones exist offshore in the jet with associated downwelling velocities of the order of 10 m d^{-1}. Vertical velocities of the order of 20 m d^{-1} and larger which result from changes in relative vorticity are reported by Swenson et al. (1990) from clusters of drifters deployed in the jet. Persistent vertical velocities of this same magnitude are found in the vorticity and vertical velocity analysis of Dewey et al. [this issue]. Another mechanism that could lead to water mass subduction is the interaction of the jet with a large-scale deformation field. The resulting ageostrophic, cross-jet transport leads to downwelling on the cyclonic side of the jet [*Onken* et al., 1990]. Numerical modeling experiments for the CTZ area also result in downward vertical velocities consistent with our observations [Hofmann et al., this issue].

Two important issues concerning the impact of subduction processes on the circulation in this coastal transition zone are the total volume of subducted water and the vertical volume flux. A lower bound on the subducted volume in the jet may be estimated by assuming that the fraction of all profiles in the jet satisfying the subduction criteria developed in section 4 is representative of the jet volume as a whole. During leg 2 of the Washington cruise, a total of 50 profiles were obtained in the jet (i.e., 51500 dbar dynamic height in the range 0.82–0.96 m) and just over 1% of all the water column from these profiles satisfy the criteria. The total volume of the jet above 500 m in the survey area is about 9000 km^3, so the subducted volume is of the order of 100 km^3. Assuming that the total subducted volume is transported out the jet axis in 12 to 21 days (the transit times on the 25.8 isopycnal from Table 1) and that a steady state volume of subducted water is maintained in the jet, the required vertical volume flux is of the order of 5 to 8 km^3 d^{-1}. An estimate of the vertical mass flux of chlorophyll may be made using the average fluorescence level in the subducted layers and a chlorophyll calibration derived for the depth range from the 1% light level to 150 m (separate analysis by B. H. Jones). The mean chlorophyll concentration is about 1 mg/l and the resulting vertical mass flux of chlorophyll is of the order of (5–9) x 10^3 kg d^{-1}.

The subducted volume estimate of 100 km^3 is likely an underestimate for the study area as a whole, possible by as much as an order of magnitude, for two reasons. First, the depth criterion of 120 m is very conservative, since it is based on the deepest 0.1% light level in the clearest offshore waters. If this criterion is relaxed to, say, the average 0.1% light level found in the jet, about 83 m, then the fraction of the water column satisfying the subduction criterion would be 4 times larger on the basis of Figure 3*b*. (This average

0.1% light level is based on analysis, not presented here, by B. H. Jones.) Second, only about one third of the stations from all of the grid surveys showing evidence of subduction is found in the jet (Figure 4). Combining these factors, the total subducted volume in the entire study area may be as large as 1000 km^3, and if the vertical processes leading to subduction have similar rates inside and outside the jet, the vertical volume flux might be as much as 80 $km^3\ d^{-1}$. The corresponding vertical mass flux of chlorophyll in this case would be of the order of 9×10^4 kg d^{-1}. For illustration, the areas of a 50-m-deep euphotic zone which would be subducted by vertical volume fluxes of 5 and 80 $km^3\ d^{-1}$ are indicated by squares in Figure 5. The larger square is 40 km on a side. Clearly, more observations are required to constrain the subducted volumes and rates and to determine the impacts of subduction processes on coastal circulation and ecology.

Acknowledgments. Ken Brink and Dave Mackas provided helpful comments on an early draft of the manuscript, and Jane Huyer kindly supplied CTD data. This work was supported by the Office of Naval Research, Coastal Sciences Program.

REFERENCES

Anderson, G. G., Subsurface chlorophyll maximum in the northeast Pacific Ocean, ***Limnol. Oceanogr.,*** 14, 386391, 1969.

Baker, E. T., and J. W. Lavelle, The effect of particle size on the light attenuation coefficient of natural suspension, ***J. Geophys. Res.,*** *89*(C5), 8197–8203, 1984.

Beers, J. R., F. M. H. Reid, and G. L. Stewart, Microplankton of the North Pacific central gyre, Population structure and abundance, June 1973, ***Int. Rev. Gesamten Hydrobiol.,*** 60, 607–638, 1975.

Bienfang, P., Sedimentation of suspended microparticulate material in the Pt. Conception upwelling ecosystem, Technical Report, 24 pp., The Oceanic Inst., Waimanolo, Hawaii, 1985.

Bienfang, P. K., Sinking rate dynamics of ***Cricosphaera carterae*** Braarud, 1, Effects of growth rate, limiting substrate, and diurnal variations in steady-state populations, ***J. Exper. Mar. Biol. Ecol.,*** 49, 217–233, 1981.

Bienfang, P., and J. Szyper, Effects of temperature and salinity on sinking rates of the centric diatom ***Ditylum brightwelli, Biol. Oceanogr.,*** *1*(3), 211–223, 1982.

Bienfang, P., J. Szyper, and E. Laws, Sinking rate and pigment responses to light-limitation of a marine diatom: Implications to dynamics of chlorophyll maximum layers, ***Oceanol. Acta,*** *6*(1), 55–62, 1982.

Bishop, J. K. B., The correction and suspended particulate matter calibration of Sea Tech transmissometer data, ***Deep Sea Res.,*** *33*(1), 121–134, 1986.

Bower, A. S., and T. Rossby, Evidence of cross-frontal exchange processes in the Gulf Stream based on isopycnal RAFOS float data, ***J. Phys. Oceanogr.,*** *19*(9), 1177–1190, 1989.

Brink, K. H., R. C. Beardsley, P. P. Niiler, M. Abbott, A. Huyer, S. Ramp, T. Stanton, and D. Stuart, Statistical properties of near-surface flow in the California coastal transition zone, ***J. Geophys. Res.,*** this issue.

Cullen, J. J., The deep chlorophyll maximum: Comparing vertical profiles of chlorophyll ***a, Can. J. Fish. Aquat. Sci.,*** 39, 791–803, 1982.

Davis, R. E., Drifter observations of coastal surface currents during CODE: The statistical and dynamical views, ***J. Geophys. Res.,*** *90*(C3), 4756–4772, 1985.

Dewey, R. K., J. N. Moum, C. A. Paulson, D. R. Caldwell, and S. D. Pierce, Structure and dynamics of a coastal filament, ***J. Geophys. Res.,*** this issue.

Flament, P. J., L. Armi, and L. Washburn, The evolving structure of an upwelling filament, ***J. Geophys. Res.,*** *90*(C6), 11,765–11,778, 1985.

Herbland, A., and B. Voituriez, Hydrological structure analysis for estimating the primary production in the tropical Atlantic Ocean, ***J. Mari. Res.,*** 37, 87–101, 1979.

Hofmann, E. E., K. S. Hedstrom, J. R. Moisan, D. B. Haidvogel, and D. L. Mackas, The use of simulated drifter tracks to investigate general transport patterns and residence times in the coastal transition zone, ***J. Geophys. Res.,*** this issue.

Hood, R., Phytoplankton biomass, photosynthetic light response, and physical structure in a norther" California upwelling system, Ph.D. dissertation, Scripps Inst. of Oceanogr., La Jolla, 1990.

Huyer, A., P. M. Kosro, J. Fleischbein, S. R. Ramp, T. Stanton, L. Washburn, F. P. Chavez, T. J. Cowles, and R. L. Smith, Currents and water masses of the coastal transition zone off northern California, June to August 1988, ***J. Geophys. Res.,*** this issue.

Jackson, G., A model of formation of marine algol flocs by physical coagulation processes, ***Deep Sea Res.,*** in press, 1991.

Jerlov, H. G., ***Marine Optics,*** 231 pp., Elsevier, New York, 1976.

Kadko, D. C., L. Washburn, and B. H. Jones, Evidence of subduction within cold filaments of the northern California coastal transition zone, ***J. Geophys. Res.,*** this issue.

Kiefer, D. A., Fluorescence properties of natural phytoplankton populations, ***Mar. Biol.,*** 22, 263–269, 1973.

Onken, R., J. Fischer, and J. D. Woods, Thermohaline finestructure and its relation to frontogenesis dynamics, ***J. Phys. Oceanogr.,*** *20*(9), 1379–1394, 1990.

Pak, H., and J. R. V. Zaneveld, Bottom nepheloid layers and bottom mixed layers observed on the continental shelf off Oregon during the upwelling season, ***J. Geophys. Res.,*** 82, 3921–3931, 1977.

Prezelin, B. B., Light reactions in photosynthesis, Physiological bases of phytoplankton ecology, ***Can. Bull. Fish. Aquat. Sci.,*** 210, 1–43, 1981.

Smayda, T. J., The suspension and sinking of phytoplankton in the sea, ***Oceanogr. Mar. Biol., 8,*** 353–414, 1970.

Smetacek, V. S., Role of sinking in diatom life-history cycles: Ecological, evolutionary, and geological significance, ***Mar. Biol.,*** 84, 239–251, 1985.

Spinrad, R. W., A calibration diagram of specific beam attenuation, ***J. Geophys. Res., 91***(C6), 7761–7764, 1986.

Strub, P. T., et al., The nature of the cold filaments in the California Current system, ***J. Geophys. Res.,*** this issue.

T. Cowles and P. M. Kosro, College of Oceanography, Oregon State University, Corvallis, OR 97331.

T. Hayward, Scripps Institution of Oceanography, University of California, San Diego, La Jolla, CA 92093.

B. H. Jones, Hancock Institute for Marine Studies, University of Southern California, Los Angeles, CA 90089.

D. C. Kadko, Rosenstiel School for Marine and Atmospheric Science, University of Miami, 4600 Rickenbacker Causeway, Miami, FL 33149.

S. Ramp, and T. P. Stanton, Department of Oceanography, Naval Postgraduate School, Monterey, CA 93943.

L. Washburn, Department of Geography, University of California, Santa Barbara, CA 93106.

(Received July 9, 1990;
accepted March 25, 1991.)